



저작자표시-비영리-변경금지 2.0 대한민국

이용자는 아래의 조건을 따르는 경우에 한하여 자유롭게

- 이 저작물을 복제, 배포, 전송, 전시, 공연 및 방송할 수 있습니다.

다음과 같은 조건을 따라야 합니다:



저작자표시. 귀하는 원저작자를 표시하여야 합니다.



비영리. 귀하는 이 저작물을 영리 목적으로 이용할 수 없습니다.



변경금지. 귀하는 이 저작물을 개작, 변형 또는 가공할 수 없습니다.

- 귀하는, 이 저작물의 재이용이나 배포의 경우, 이 저작물에 적용된 이용허락조건을 명확하게 나타내어야 합니다.
- 저작권자로부터 별도의 허가를 받으면 이러한 조건들은 적용되지 않습니다.

저작권법에 따른 이용자의 권리는 위의 내용에 의하여 영향을 받지 않습니다.

이것은 [이용허락규약\(Legal Code\)](#)을 이해하기 쉽게 요약한 것입니다.

[Disclaimer](#)

Study on advanced electrolyte
for improving electrochemical performance
of lithium-sulfur batteries

The background features a large, light gray watermark of the UNIST logo. It consists of a circular emblem with the text 'UNIST NATIONAL INSTITUTE OF SCIENCE AND TECHNOLOGY' around the perimeter. Inside the circle is a stylized 'U' shape, and within that, a globe with orbital lines.

Jin-Tak Yeon

Battery Science and Technology Program
Graduate School of UNIST

2013

Study on advanced electrolyte
for improving electrochemical performance
of lithium-sulfur batteries

Jin-Tak Yeon

Battery Science and Technology Program
Graduate School of UNIST

Study on advanced electrolyte
for improving electrochemical performance
of lithium-sulfur batteries

A thesis
submitted to the Graduate School of UNIST
in partial fulfillment of the
requirements for the degree of
Master of Science

Jin-Tak Yeon

02.05.2013 Month/Day/year of submission

Approved by

A handwritten signature in black ink, reading "Nam-Soon Choi", is written over a horizontal line.

Major Advisor
Nam-Soon Choi

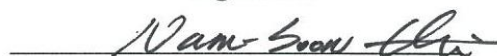
Study on advanced electrolyte
for improving electrochemical performance
of lithium-sulfur batteries

Jin-Tak Yeon

This certifies that the thesis of Jin-Tak Yeon is approved.

02.05.2013 Month/Day/year of submission

signature



Thesis supervisor: Nam-Soon Choi

signature



Kyu-Tae Lee

signature



Soo-Jin Park

Abstract

Lithium-sulfur (Li-S) batteries have been drawing attention as one of the high density energy storage devices due to their high theoretical capacity ($1,672\text{mAh g}^{-1}$), high theoretical energy density (2600Wh kg^{-1}), which is 3 to 5 times higher than that of Li ion batteries based on intercalation reactions, eco-friendliness and low cost. In spite of these advantages, there are many problems that hinder practical applications. The challenges are attributed to the solubility of the polysulfide ions (S_n^{2-}) formed on electrochemical reduction of S_8 or on electrochemical oxidation of insoluble sulfides. In the first discharge step, electrochemical conversion of S_8 to form S_4^{2-} occurs through a sequence of soluble molecular poly-sulfides. The formation of insoluble Li_2S_2 is hindered and conversion of Li_2S_2 to Li_2S as the last discharge step is the most difficult. In addition, Li metal as an anode in Li-S batteries is problematic when it is contact with any kind of liquid electrolyte solution, because of its high reactivity. Li metal would result in poor cycling efficiencies due to the severe growth of the SEI layer and Li dendrite formation. Moreover, insulating products layer such as Li_2S and Li_2S_2 on Li anode can be formed by the reaction of Li and soluble polysulfide intermediates Li_2S_n ($4 \leq n \leq 6$), which are diffused from the cathode.

This study is concerned with the understanding and the improvement of Li-S battery. In order to understand basic operation mechanism of Li-S battery, structural evolution of sulfur cathode and lithium anode was investigated by using Raman spectroscopy and X-ray diffraction during discharge and charge. With based on such understanding, the improvement of Li-S battery was also performed by using protection layer with FEC based electrolytes .

The effect of solvents on the discharge behavior of Li-S cells was investigated by ex situ Raman spectroscopy and X-ray diffraction. Lithium polysulfide species formed in a sulfur cathode during cycling are characterized by Raman experiments for the first time and their structures are examined with regard to three different electrolytes at fully charged and discharged states. Moreover, ex-situ Raman studies give the evidence for the formation of lithium polysulfide on a Li metal anode by shuttle phenomena and the coexistence of soluble lithium polysulfide with elemental sulfur even after full charge. It was found that 1,3-dioxolane (DOX)/1M LiTFSI facilitates the migration of soluble lithium polysulfide toward a lithium anode and initiates a polysulfide shuttle causing a considerable capacity loss in Li-S cells. Raman results and cycling tests using an air-tight cell demonstrated that tetra(ethylene glycol) dimethyl ether (TEGDME)-based electrolytes hindered the significant overcharge and led to the formation of Li_2S_2 contributing to high discharge capacity through further electrochemical reduction to Li_2S .

In addition, the impact of a fluoroethylene carbonate (FEC) solvent on the electrochemical performance of Li-Li and Li-S cells was investigated. To confirm the effects of FEC on electrolyte

decomposition and cell resistance, the surface chemistry and impedance of a Li electrode cycled in electrolytes with and without a FEC solvent were investigated using attenuated total reflectance–Fourier transform infrared (ATR-FTIR) spectroscopy, X-ray photoelectron spectroscopy (XPS), time of flight secondary ion mass spectrometry (ToF-SIMS), and electrochemical impedance spectroscopy. It is found that the protective layer with FEC hinders the migration of soluble lithium polysulfides toward a Li metal electrode and results in the suppression of overcharging of Li-S cells.

Contents

CHAPTER I	1
1. Introduction	1
2. Research objectives	5
CHAPTER II. Raman Spectroscopic and X-ray Diffraction Studies of Sulfur Composite Electrodes during Discharge and Charge	7
1. Introduction	7
1.1. History of lithium sulfur battery	7
1.2. Electrochemical reaction mechanism of lithium sulfur battery	11
1.3. Research objectives	14
2. Experimental	15
2.1. Preparation of lithium sulfur cell	15
2.2. Electrical properties measurements	15
2.3. Raman spectroscopy	15
2.4. X-ray diffraction (XRD)	16
2.5. Focused Ion Beam (FIB) & Energy Dispersive Spectrometer (EDS)	16
2.6. ⁷ Li NMR	16
3. Results and Discussion	18
3.1. Images of sulfur cathodes	18
3.2. Charge/discharge characteristics of lithium sulfur cell	18
3.3. The effect of ether-based solvents on electrochemical performance	27
4. Conclusions	33
CHAPTER III. Effect of fluoroethylene carbonate on electrochemical performances of lithium electrodes and lithium-sulfur batteries	34
1. Introduction	34
1.1. Rechargeable Lithium Anode	34
1.2. Intrinsic Properties of Lithium Metal Electrode and Approaches for its Stabilization	35
1.3. Lithium metal electrode/ electrolyte interface	40
1.3.1. SEI model I : Homogeneous layers	40
1.3.2. SEI model II : Composite and Stratified layers	40
1.4. Protection layer on Li metal	43
1.5. Research objectives	43

2. Experimental	44
2.1. Preparation of lithium sulfur cell	44
2.2. Electrical properties measurements	45
2.3. Characterization of Li metal after dissolution & deposition.....	46
2.4. Preparation of lithium and protected lithium anodes	46
3. Results and Discussion	48
3.1. Effect of TEGDME on Li metal	48
3.2. Effect of FEC based electrolyte on lithium deposition/dissolution process in Li symmetric cell	48
3.3. Effect of protection layer on charge & discharge performance of Li-S cell	56
4. Conclusions	61
References	62

LIST OF FIGURES

Figure 1. Schematic description of a “(lithium ion) rocking- chair” cell that employs graphitic carbon as anode and transition metal oxide as cathode.

Figure 2. (a) Schematic illustration of a typical Li-S cell. (b) A typical voltage vs capacity plot for a Li-S cell.

Figure 3. Energy source requirement.

Figure 4. Representative charge/discharge curves for a lithium sulfur cell.

Figure 5. Picture of an air-tight cell for ex-situ Raman measurements. (a) Cell body. (b) Bottom of (a) with glass window that laser beam enters.

Figure 6. (a), (b) The cross-section images of sulfur composite cathodes and EDS spectra for (c) selected zone 1 and (d) selected zone 2.

Figure 7. First discharge and charge profiles of a Li-S cell between 1.5 and 2.8 V vs. Li/Li⁺ at a current density of 83.6 mA g⁻¹ (C/20).

Figure 8. Optical microscope images showing the sulfur composite cathode surface at various discharged and charged states. (a) Pristine cathode. (b) Discharged to 2.28 V. (c) Discharged to 2.1 V. (d) Full discharge. (e) Charged to 2.34 V. (f) Charged to 2.4 V. (g) Full charge.

Figure 9. Raman spectra of sulfur cathodes obtained from seven representative points of Fig. 3. (a) Pristine cathode. (b) Discharged to 2.28 V. (c) Discharged to 2.1 V. (d) Full discharge. (e) Charged to 2.34 V. (f) Charged to 2.4 V. (g) Full charge.

Figure 10. XRD patterns of the sulfur composite cathodes. (a) Li₂S powder. (b) Pristine sulfur cathode. (c) Fully discharged cathode without washing. (d) Fully discharged cathode with washing. (e) Fully charged cathode without washing.

Figure 11. Raman spectra of Li metal anodes. (a) Before cycle. (b) After full discharge. (c) After full charge.

Figure 12. Comparison of discharge and charge profiles for a Li-S cell with a different electrolyte at a current density of 83.6 mA g⁻¹ (C/20).

Figure 13. Raman spectra measured from the sulfur cathodes after (a) Fully discharged in TEGDME/1M LiTFSI. (b) Fully charged in TEGDME/1M LiTFSI. (c) Fully discharged in TEGDME/DOX (40/60) 1M LiTFSI. (d) Fully charged in TEGDME/DOX (40/60) 1M LiTFSI. (e) Fully discharged in DOX/1M LiTFSI. (f) Fully charged in DOX/1M LiTFSI. (g) Enlarged spectra of (f).

Figure 14. An optical microscope images showing the sulfur composite cathode surface after (a) Full discharge in DOX/1M LiTFSI. (b) Charged up to 710 mAh g⁻¹ in DOX/1M LiTFSI (Compulsory capacity cutoff). (c) Full discharge in TEGDME/1M LiTFSI. (d) Full charge in TEGDME/1M LiTFSI.

(e) Schematic drawing for reaction pathway in DOX- or TEGDME-based electrolytes. (f) SEM image of the cross section of a sulfur cathode fully discharged in TEGDME/DOX/1M LiTFSI with EDS spectrum. (g) SEM image of the cathode surface fully discharged in TEGDME/DOX (40/60) 1M LiTFSI.

Figure 15. Schematic illustration for the formation and growth of SEI layer on the lithium electrode.

Figure 16. Schematic illustration for the formation of dendritic lithium on the lithium electrode.

Figure 17. Modification history for stabilization of the lithium metal electrode

Figure 18. Different interphase model of the lithium electrode/organic electrolyte Interface

Figure 19. (a) Schematic drawing for the formation and roles of a protective layer on the Li electrode via UV irradiation. (b) SEM image of a protective layer. (c) A Li-S cell with a protective layer.

Figure 20. Galvanostatic cycling performance of Li symmetrical cells in TEGDME/1M LiPF₆ at a rate of C/10 during first Li dissolution from the Li electrode.

Figure 21. Galvanostatic cycling performance of Li symmetrical cells in Ref and FEC60 electrolytes at a rate of C/10 (a) during 10 cycles. (b) during 80 cycles. The inset is the enlarged zone from 60 to 80 cycles. 25% of Li from the Li counter electrode migrates to the Li working electrode in the Li/electrolyte/Li cell during Li deposition. (c) Impedance spectra of Li symmetrical cells after 5 cycles, (d) Impedance spectra of Li symmetrical cells after 10 cycles.

Figure 22. SEM images of the Li electrode surface after Li dissolution in (a) Ref. (b) FEC60, after Li deposition in (c) Ref. (d) FEC60.

Figure 23. ATR-FTIR spectra of the Li electrode surface after Li dissolution in two electrolyte solutions.

Figure 24. F1s high-resolution XPS spectra of surface films formed on Li electrode surface after Li dissolution in (a) Ref, (b) FEC60 at 30°C. Red lines are curve fitting results.

Figure 25. ToF-SIMS F⁻ ion maps of the Li electrode surface after dissolution in (a) Ref, (b) FEC60.

Figure 26. Electrochemical performance of the Li-S cells during galvanostatic cycling at 30°C. (a) Voltage profiles, (b) Coulombic efficiency, (c) Discharge capacity.

Figure 27. SEM images of the surface of the protection layer with (a) TEGDME electrolyte, (b) FEC60 electrolyte. EDS mapping results for the surface of the protection layer with (a) TEGDME electrolyte, (b) FEC60 electrolyte.

Figure 28. SEM images and EDS spectra of non-protected Li and protected Li surface .

LIST OF TABLES

Table 1. Comparison of a typical C/Li[Co_{1/3}Ni_{1/3}Mn_{1/3}]O₂ battery and the Li-S battery.

Table 2. Composition of various electrolytes.

Table 3. Composition of protection layers formed on the Li electrode surface in Li-S cells.

CHAPTER I

1. Introduction

The rapid proliferation of innovative technologies and growing environmental concerns have created immense interest in the development of more efficient, pollution free, and safe energy sources. The growing concern over global warming and air pollution has triggered the replacement of nonrenewable energy sources such as petroleum by alternative energy source. Electrochemical energy storage systems play important role on use of intermittent renewable energy generation such as wind, solar, wave plants and reduction in the consumption of fossil fuels for transportation.

Among many energy-storage systems, Lithium batteries will perform an increasing crucial role due to their high specific energy (energy per unit weight) and energy density (energy per unit volume). Current lithium ion (Li-ion) batteries have been widely used in consumer electronic devices especially for cellular phones and portable computers.¹⁻⁴ Conventional Li ion batteries (LIB`s) utilize a transition metal oxide or phosphate with a crystalline structure as a cathode and graphitized carbon with interlayer structure as a anode where Li ions intercalate into or de-intercalate between two electrodes, which is called “rocking-chair battery”.⁵⁻⁶ (Fig. 1)

However, although Li ion batteries are fully developed the highest energy of LIB`s has limitation below 250Wh kg⁻¹ and 800Wh L⁻¹. The numerical value is too low to meet the demands of transportation markets, particularly for full scale electrical vehicles (EV). In case of EV, it requires advanced high capacity batteries that can produce competitive long range above 500km. To satisfy the requirement, new chemistry must be brought in for especially electrochemistry and new materials, which potentially can be realized through redox-driven phase-transformation chemistry that involves sulfur or oxygen as cathodes. These future generation systems offer increased energy densities, reduced cost factors, and more benign environmental factors due to their use of nontoxic elements.

Sulfur has many valuable characteristics, such as low equivalent weight, extremely low cost, and environmentally benign.⁷ Sulfur is a promising cathode for lithium batteries because its chemistry is vastly different from that which governs typical intercalation materials (i.e., LiFePO₄, LiMn₂O₄). In its most stable form, sulfur forms a molecular structure with a density of 2.07 g cm⁻³ comprised of stacked eight atom rings (S₈), which expands during discharge owing to the lower density of Li₂S (1.67 g cm⁻³), and contracts again on charge. In typical lithium-sulfur (Li-S) cells (Fig. 2a), lithium metal, of which theoretical specific capacity is 3600mAh g⁻¹, is used as the negative electrode and is separated from the positive sulfur electrode by an ion conducting liquid or solid electrolyte. During discharge of the cell, the sulfur-sulfur bonds are cleaved to open the S₈ ring, and subsequent shortening of the sulfur chain length is thought to occur as shown in Fig. 2b.

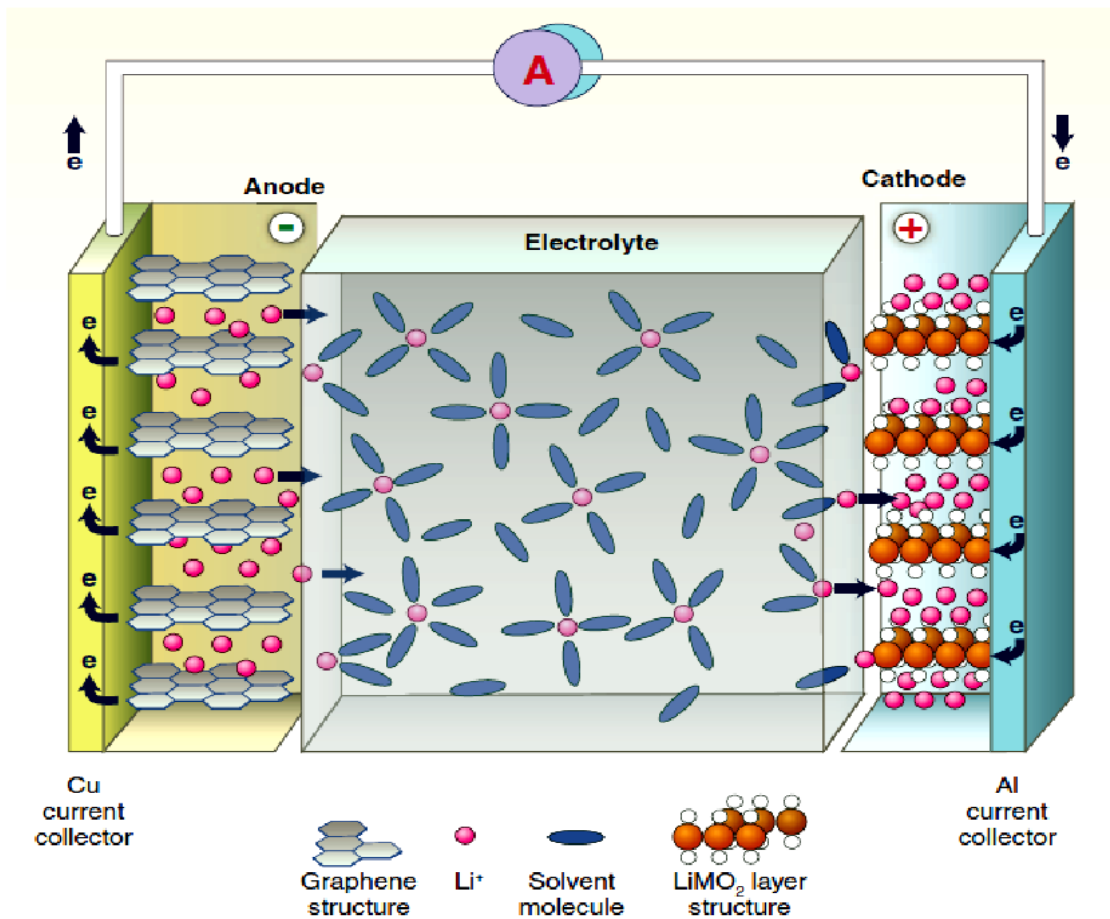
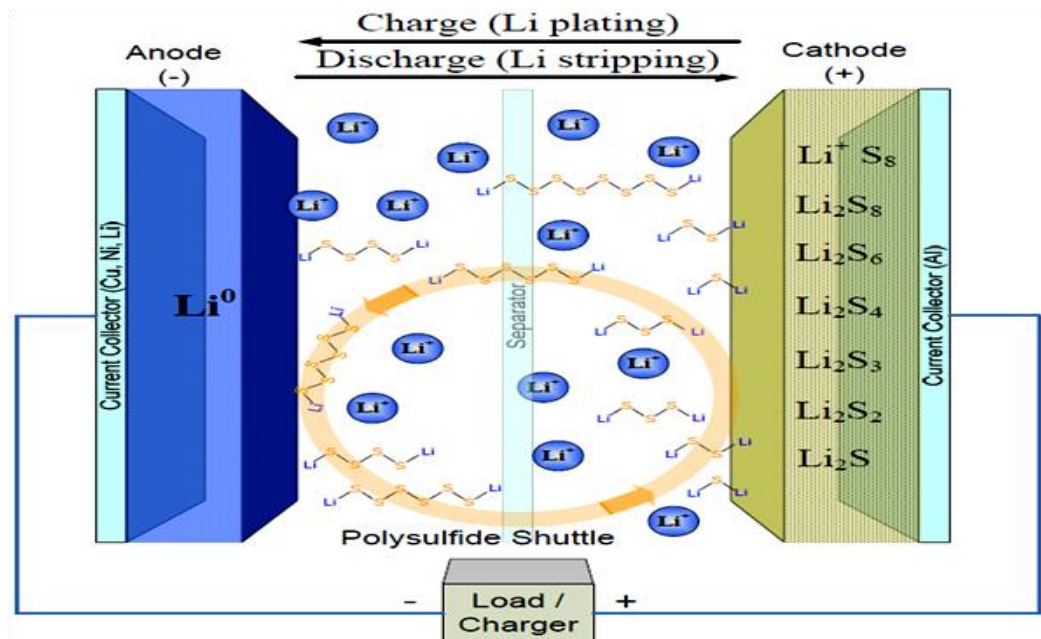


Figure 1. Schematic description of a “(lithium ion) rocking- chair” cell that employs graphitic carbon as anode and transition metal oxide as cathode.

(a)



(b)

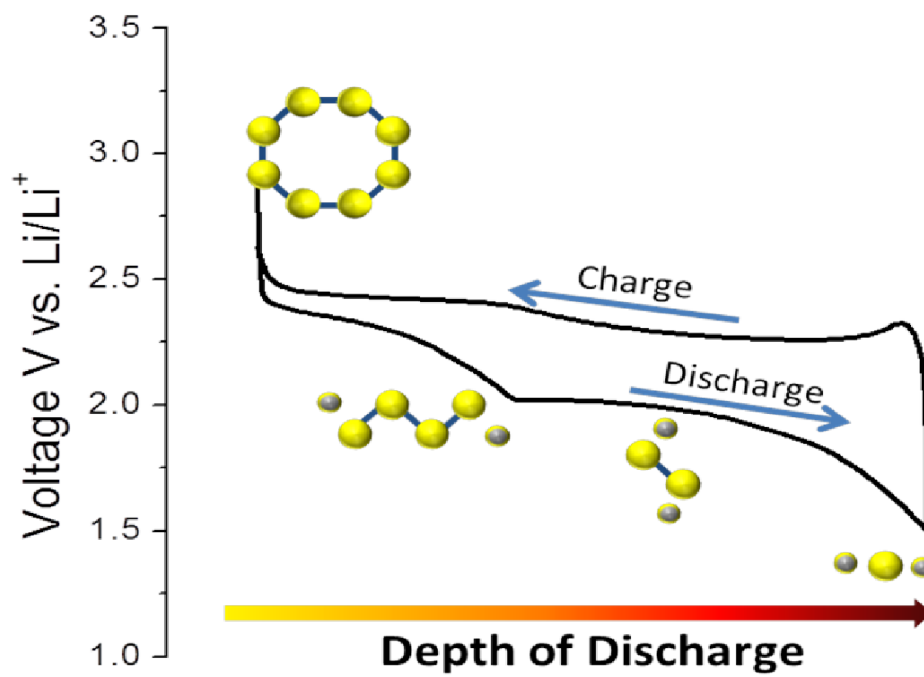


Figure 2. (a) Schematic illustration of a typical Li-S cell. (b) A typical voltage vs capacity plot for a Li-S cell.

The overall redox couple of a Li-S cell is described by the reaction $S_8 + 16Li \rightarrow 8Li_2S$ and occurs at a potential of 2.15V vs Li/Li⁺, which is about 1/2 to 2/3 lower than typical intercalation transition metal oxide electrode materials. This lower potential is not detrimental for practical applications because the gravimetric capacity of sulfur is the highest of any solid cathode material at 1672mAh g⁻¹. It correlates to theoretical energy densities of 2600Wh kg⁻¹ based on weight, which is a factor of 3 ~ 5 times higher than any that value for any other commercial lithium ion cell at a significantly lower cost.⁸⁻¹⁸

Despite these advantages, massive implementation of Li-S batteries remains hindered by several serious challenges, including low utilization of sulfur active material, low coulombic efficiency and rapid capacity loss during cycling. The major problem is rapid capacity fading, which is mainly due to dissolution of long chain polysulfide anion (S_n²⁻)-intermediate reaction species formed on charge and discharge-from the cathode into the electrolyte.¹⁹ Moreover, the low electronic conductivity of sulfur (5×10^{-30} S/cm at 25°C)²⁰ and polysulfide inhibit the complete reaction of sulfur active materials to Li₂S. In the first discharge step, the electrochemical conversion of S₈ to form S₄²⁻ occurs through a sequence of soluble molecular polysulfide. The formation of insoluble Li₂S₂ is hindered and the conversion of Li₂S₂ to Li₂S as the last discharge step is the most difficult.¹⁹ In addition, Insoluble agglomerates are thus formed on the surface over prolonged cycling regardless of the initial cathode morphology.^{21,22} In a typical Li-S cell, elemental sulfur serves as the active material of the cathode, which undergoes reduction via a series of polysulfides, Li₂S_n (n = 2 ~ 8), to ultimately form Li₂S during discharge. The long chain polysulfide ions S_n²⁻ formed in the cathode during discharge are soluble in the electrolyte, and diffuse through the separator to the anode, where they are reduced to insoluble Li₂S₂ or Li₂S.²³⁻²⁵ Once the lithium anode is fully coated, the diffused S_n²⁻ reacts with these reduced sulfides to form lower order polysulfides that become concentrated at the anode and then diffuse back to the cathode and are re-oxidized to S_n²⁻. The above shuttle process takes place repeatedly, causing a decrease of active material at the cathode, capacity fading, inactivation of the anode, and self-discharge of the cell.²⁶ Finally, dendrite formation on the Li electrode during the Li deposition, which can cause short-circuits, and undesirable reaction of the Li electrode with the electrolyte solution should be overcome.

White group presented a mathematical model for valuable reaction mechanism of sulfur on the discharge of Li-S batteries.²⁷ However, there has been no clear reasoning of the problems mentioned above due to the lack of the understanding on the definite mechanism of the property changes in the sulfur cathode and the lithium anode during electrochemical process.

2. Research objectives

Despite three decades of research on Li-S batteries, the mechanism of the Li-S cell is still controversial. As many polysulfide species are known to exist in solution, different sulfur reduction mechanisms could be found in the literature, and the authors do not agree about the intermediate species that would be occurred during the electrochemical process.

There are several major issues facing rechargeable Li-S batteries that impede their practical applications; a low utilization of active material, poor cycle life, and low system efficiency. To solve these problems, a variety of strategies have been applied to Li-S cell for the enhancement of the electrochemical performance. The majority of approaches have been carried out by forming sulfur composites with favorable structures and properties at a cathode. Other approaches have been dealt with by modifying anode materials and using efficient electrolytes.

In this dissertation, the understanding of Li-S battery operating mechanism and the improvement of Li-S battery were performed. As described above, the understanding on the properties changes of the cathode and anode is highly required for further improvement of the Li-S battery. In order to clarify detailed operation mechanism of Li-S battery, the intermediate product species formed in sulfur cathode and lithium anode were investigated during discharge and charge. Furthermore, the discharge and charge capacities of Li-S cells with different electrolytes were also investigated. Herein, we present the effect of solvents on electrochemical conversion of S_8 during the first Li insertion by means of in-situ Raman and ex-situ XRD studies.

Another main objective of this study is to enhance the charge/discharge performance by reducing the growth of the SEI layer and suppressing the reaction between the Li and soluble polysulfides. We tried to design the protective thin layer on Li anode by prepared by a UV cured polymerization method. In addition, the impact of a fluoroethylene carbonate (FEC) solvent on the electrochemical performance of Li-Li and Li-S cells is investigated. To confirm the effects of FEC on electrolyte decomposition and cell resistance, the surface chemistry and impedance of an Li electrode cycled in electrolytes with and without a FEC solvent are investigated using attenuated total reflectance–Fourier transform infrared (ATR-FTIR) spectroscopy, X-ray photoelectron spectroscopy (XPS), time of flight secondary ion mass spectrometry (ToF-SIMS), and electrochemical impedance spectroscopy.

In Chapter II, a detailed description of the intermediate product species formed in sulfur cathodes was investigated at various discharged and charged states. An evidence for the migration of soluble lithium polysulfide toward Li metal anode was proved by means of an air-tight Raman cell and ex-situ XRD. Additionally, the influence of ether-based solvents, which show different viscosity, on electrochemical reduction and oxidation of elemental sulfur was dealt with on the basis of Raman studies. The discharge and charge capacities of Li-S cells with different electrolytes were also

investigated.

In Chapter III, the effect of FEC on the dissolution and deposition of Li metal was studied during galvanostatic cycling of lithium symmetrical cells. In order to retard the movement of soluble polysulfides toward an Li electrode and stabilize the Li metal electrode more effectively, the protective polymer film physically separated with bulk electrolyte is formed on the Li electrode of a Li-S cell. To the best of our knowledge, we first demonstrate the significant role of a polymer thin film with FEC in electrochemical performances of Li-S batteries using attenuated total reflectance–Fourier transform infrared (ATR-FTIR) spectroscopy, X-ray photoelectron spectroscopy (XPS), time of flight secondary ion mass spectrometry (ToF-SIMS), and electrochemical impedance spectroscopy.

CHAPTER II

Raman Spectroscopic and X-ray Diffraction Studies of Sulfur Composite Electrodes during Discharge and Charge

1. Introduction

1.1. History of lithium sulfur battery

The development of Li-S cells was historically the outcome of a systematic investigation of thermally regenerative cells at Argonne National Laboratory and other laboratories starting in the early 1960s.²⁸ This investigation, reviewed by Cairns and Steunenberg(1973)²⁹, centered initially on bimetallic systems and later on LiH; it yielded a wealth of thermodynamic and electrochemical information of the properties of molten salts and cell materials (Cairns et al., 1967). This led to investigations of Li-Te, Li-Se, and Li-S cells. In these cells, the negative electrode consisted of porous metal (nickel or steel) in which liquid lithium was absorbed. The positive electrode consisted of the elemental chalcogen contained in a current collector of extended area to maximize contact between the collector and the poorly conducting reactant.

The obvious superiority of the Li-S couple was at first obscured by current collection problems. These were compounded by the high vapor pressure of sulfur at cell temperature (650-700K). Relatively successful operation for several hundred cycles and up to 1000hr was made possible by various cathode designs discussed by Kyle et al. (1971) and Cairns and Steunenberg (1973). Sulfur was absorbed in porous graphite, and a thin-walled enclosure of porous molybdenum, filled with electrolyte, was found to be effective in preventing sulfur loss. Some of these cells, especially those with intimate cathode mixtures of sulfur, molybdenum, and electrolyte exhibited very high capacities (Cairns et al., 1973); this might be explained by reactions involving molybdenum and by overcharge reactions producing S_2Cl_2 .

High temperature molten sodium-sulfur cells are known and described in U.S. Pat. No. 3,404,035 issued to Kummer et al.³⁰ Such cells employ a solid state separator, typically a ceramic such as an alumina. Obviously such cells must be operated at a temperature above the melting point of sodium. It also employed a positive electrode including elemental sulfur, an electronic conductor (e.g., carbon). In regard to alkali metal-sulfur systems wherein the electrodes are molten or dissolved, and the electrolyte is solid, which function in exemplary temperature ranges of 130°C to 180°C and 300°C to 350°C. DeGott mentioned that such batteries have problems, such as, progressive diminution of the

cell's capacity, appearance of electronic conductivity in the electrolyte, and problems of safety and corrosion.^{31,32} DeGott then lists problems encountered with alkali metal-sulfur battery systems wherein the electrodes are solid and the electrolyte is an organic liquid, and by extension wherein the negative electrode is solid, the electrolyte is solid, and the positive electrode is liquid. Such problems include incomplete reduction of sulfur, mediocre reversibility, weak maximum specific power (performance limited to slow discharge regimes), destruction of the passivation layer of Li_2S as a result of its reaction with dissolved sulfur leading to the formation of soluble polysulfides, and problems with the stability of the solvent in the presence of lithium.³³

And the insulating character of sulfur is a major obstacle that is difficult to overcome. DeGott³⁴ then describes preliminary electrochemical experiments with a composite sulfur electrode prepared from a slurry. The slurry was prepared by mixing the following components in acetonitrile: 46% sulfur; 16% acetylene black; and 38% (polyethylene oxide/lithium perchlorate). The resulting slurry was then deposited on a stainless steel substrate by "capillary action". From those preliminary experiments, it is clear that, even when optimizing the efficiency of the composite electrode (that is, by multiplying the triple point contacts) that elemental sulfur cannot be considered to constitute an electrode for a secondary battery, in an "all solid" format.³⁵

The early stage rechargeable lithium batteries were being developed for portable power applications. It employed solid state polymer electrolyte. Present solid-state lithium secondary battery systems are limited to a specific energy of about 120Wh kg^{-1} . It would be highly desirable to have higher specific energy value.

It would be even more desirable if solid-state batteries having practical specific energy values greater than about 150Wh kg^{-1} could operate at room temperature. It would be additionally advantageous if solid-state batteries having high specific energy and operation at room temperature could be reliably fabricated into units with reproducible performance values. According to the patent describes poly(ethyleneoxide) based solid state Li-S cells with a capacity of more than 80% of the theoretical value for a single discharge and a cell lifetime of 400cycles at 200Wh kg^{-1} of positive electrode at 80°C .^{36,37}

In lithium cells wherein a liquid electrolyte is used, leakage of the electrolyte can leave lithium exposed to the air, where it rapidly reacts with water vapor and oxygen. Substantial casing can prevent such reactions and protect users and the environment from exposure to hazardous, corrosive, flammable or toxic solvents but adds unwanted weight to the battery. A solid-state battery would greatly reduce such problems of electrolyte leakage and exposure of lithium, and would allow reducing the weight of the battery.

However, these early stage Li-S cells are limited the operating temperature by the limitation of electrolyte and electrochemical reaction control. From these properties of the first stage cell, an

application of these systems is concentrated on electric vehicle market. Recent development of Li-S system for portable small equipments is aimed to use of liquid electrolytes with porous separator to impart a operation at ambient temperature, which is based on a progress of materials and growth of knowledge for electrochemical reaction mechanism of Li-S cell.^{8, 38}

As the non-aqueous electrolyte, a mixture of organic solvents and ionic salts is typically used. Alternatively, a gel or solid polymer electrolyte containing polymers and ionic salts, and optionally organic solvents, might be utilized instead of the liquid organic electrolyte if it provides ionic conduction at room temperature.^{39, 40}

The low equivalent weight and low cost of sulfur and its non-toxicity renders it also an attractive candidate battery component. Its theoretical specific capacity is corresponding to 1672mAh g⁻¹ and in case of that lithium metal, of which theoretical specific capacity is 3600mAh g⁻¹, is used as an anode, the Li-S redox couple could generates energy density of 2600Wh kg⁻¹, which is much higher than those of today's conventional lithium batteries such as LiMn₂O₄ and LiCoO₂. Table. 1 and Fig. 3 shows comparison theoretical capacity and energy densities of varying battery system.⁴¹

Table1. Comparison of a typical C/Li[Co_{1/3}Ni_{1/3}Mn_{1/3}]O₂ battery and the Li-S battery

System	Average Discharge Potential /V	Theoretical Capacity of Cathode /mAh g ⁻¹	Practical Capacity of Cathode /mAh g ⁻¹	“Bare-bones” energy density of a full cell ^a /Wh kg ⁻¹	“Practical” specific energy density of a full cell /Wh kg ⁻¹
C-LiMO ₂ ^e	3.7	275	160	410	135-180 ^b
Li-S	2.15	1672	500-1100	950-1700	350 ^c to 700 ^d

a Based on active mass(anode+cathode) only-excluding electrolyte, separator and components.
b Reported values for full cells from various sources.
c Data reported by Sion PowerTM.
d Based on Company projections, and estimated from data
e Li[Co_{1/3}Ni_{1/3}Mn_{1/3}]O₂

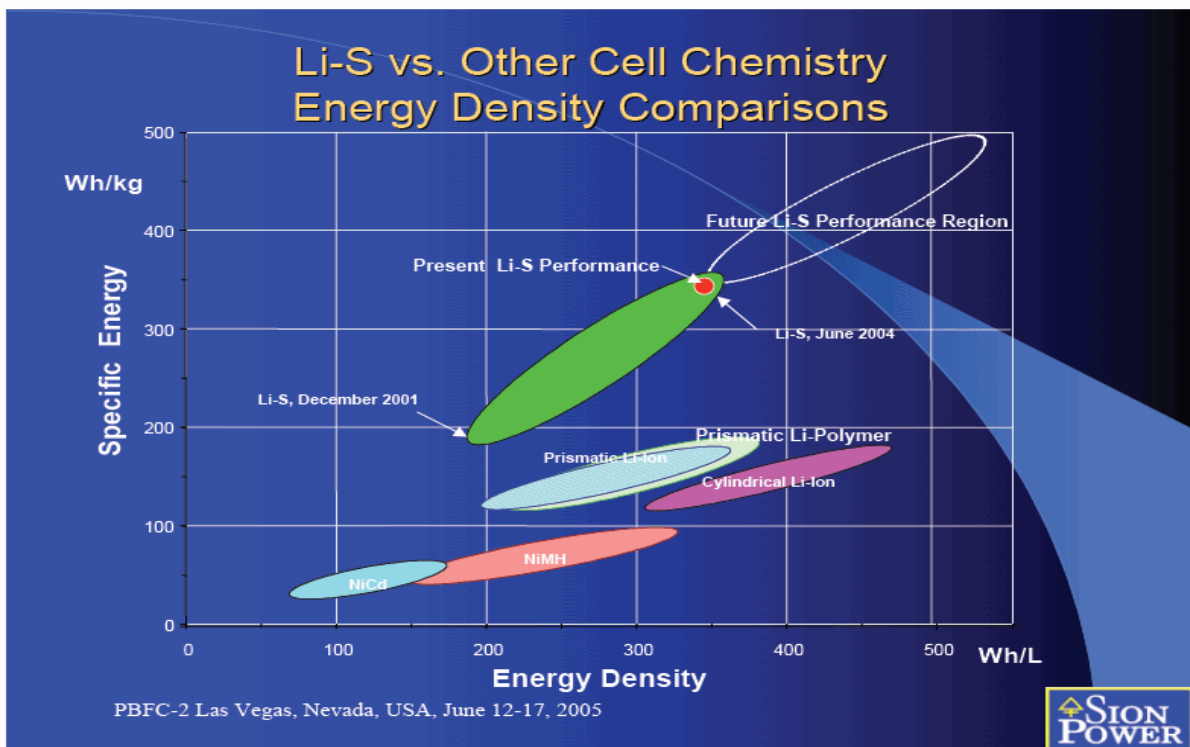


Figure 3. Energy source requirement.

1.2. Electrochemical reaction mechanism of lithium sulfur battery

The high capacity and rechargeability of sulfur are achieved from the electrochemical cleavage and reformation of sulfur-sulfur bond in cathode. These redox behaviors of sulfur and polysulfide in aprotic solvent are very complex and are not sufficiently studied. However, The earliest configuration of a Li-S battery was presented in the late 1960s.^{42,43} The positive electrode comprised elemental sulfur, electronic conductors (carbon or metal powder) and binders, separated from the metallic lithium negative electrode by an organic electrolyte. This configuration has been the platform for subsequent major research activities as well.

The parameters of Li-S batteries are dictated by the specifics of the Li-S electrochemical system. Although the positive electrode depolarizer in the fully oxidized state (elementary sulfur) and in the fully reduced state (lithium sulfide) is solid, Li-S batteries can be classified with chemical power sources with a liquid cathode: the electrochemical processes occurring in these batteries during their charge and discharge result in lithium polysulfides, which are soluble in most aprotic electrolytes.

It is known that elementary sulfur can exist in various molecular species. Elementary sulfur is soluble, although weakly, in aprotic electrolyte systems. In many cases, molecular sulfur species in solutions remain the same as in the solid phase.

The electrochemical reduction of sulfur during discharge and the oxidation of the products of its reduction during battery charge occur in two stages. This scenario is evidenced by the shape of discharge and charge curves (Fig. 4): each shows two plateaus.

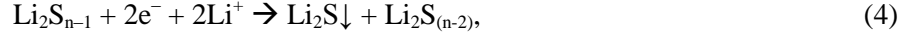
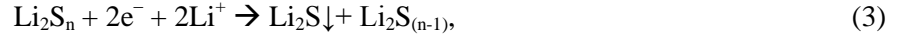
The first discharge stage of a sulfur electrode, which occurs in the potential range 2.5–2.0 V, involves the reduction of the elementary sulfur octet dissolved in the electrolyte to lithium octasulfide, which is soluble in electrolytes. Lithium octasulfides are unstable in many electrolyte systems and undergo disproportionation with the detachment of elementary sulfur, which again experiences electrochemical reduction. In a simplified form, the reduction of the elementary sulfur octet can be described by



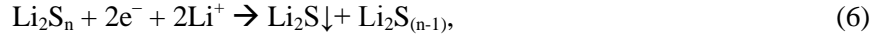
Actually, the reduction of elementary sulfur to lithium polysulfides is much more complex. Some aspects of sulfur reduction mechanisms in nonaqueous solutions are considered.^{44,45}

The second stage of lithium sulfur battery discharge involves the reduction of sulfur in lithium polysulfides dissolved in the electrolyte. The mechanism of this process is yet unclear, but we can suggest the following major schemes:

(i) the reduction of polysulfide sulfur with a systematic decrease in the polysulfide chain length and the retention of the overall lithium polysulfide concentration in the solution:



(ii) the reduction of polysulfide sulfur as a result of the rapid disproportionation of Li_2S_n , with the polysulfide chain length retained but with a systematic decrease in the overall lithium polysulfide concentration in the electrolyte solution:



Because the negative charge on sulfur atoms will increase with decreasing lithium polysulfide chain length, the redox potential of sulfur atoms will change. Therefore, if the first scheme is implemented, either separate plateaus corresponding to lithium polysulfides with certain chain lengths are expected to appear on the discharge curve, or the arrest potential will decrease systematically.

In most experiments, a single arrest appears on the discharge curve due to lithium polysulfide reduction, with the potential remaining almost unchanged to the end of the arrest. This fact provides evidence in favor of the second scheme, according to which the reduction of soluble lithium polysulfides is accompanied by their disproportionation.

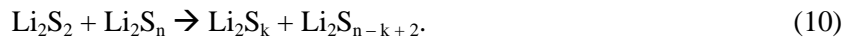
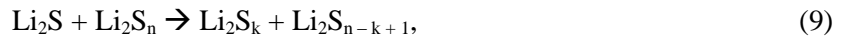
The actual mechanism of the electrochemical reduction of lithium polysulfides is more complex. Quite likely, the first or second mechanism can both be implemented depending on the composition of the electrolyte system.

The charge of Li-S batteries also occurs in two stages. First, medium-chain lithium polysulfides are reduced to long-chain ones. Roughly, the scheme of this process can be described by

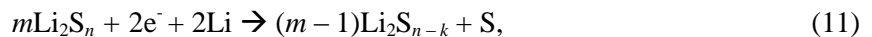


where $m k = g n$.

The resulting long-chain lithium polysulfides enter the reaction with sparingly soluble short-chain lithium polysulfides, producing medium-chain polysulfides (Eqs. (9) and (10)); the latter are again oxidized to long chain lithium polysulfides (Eq. (8)):



This process continues until sparingly soluble lithium polysulfides localized in the reaction zone are fully consumed. After this process is over, long-chain polysulfides are reduced to elementary sulfur in the potential range 2.4–2.6 V relative to the lithium electrode:



where $(mn) = (m-1)((n-k)+1)$.

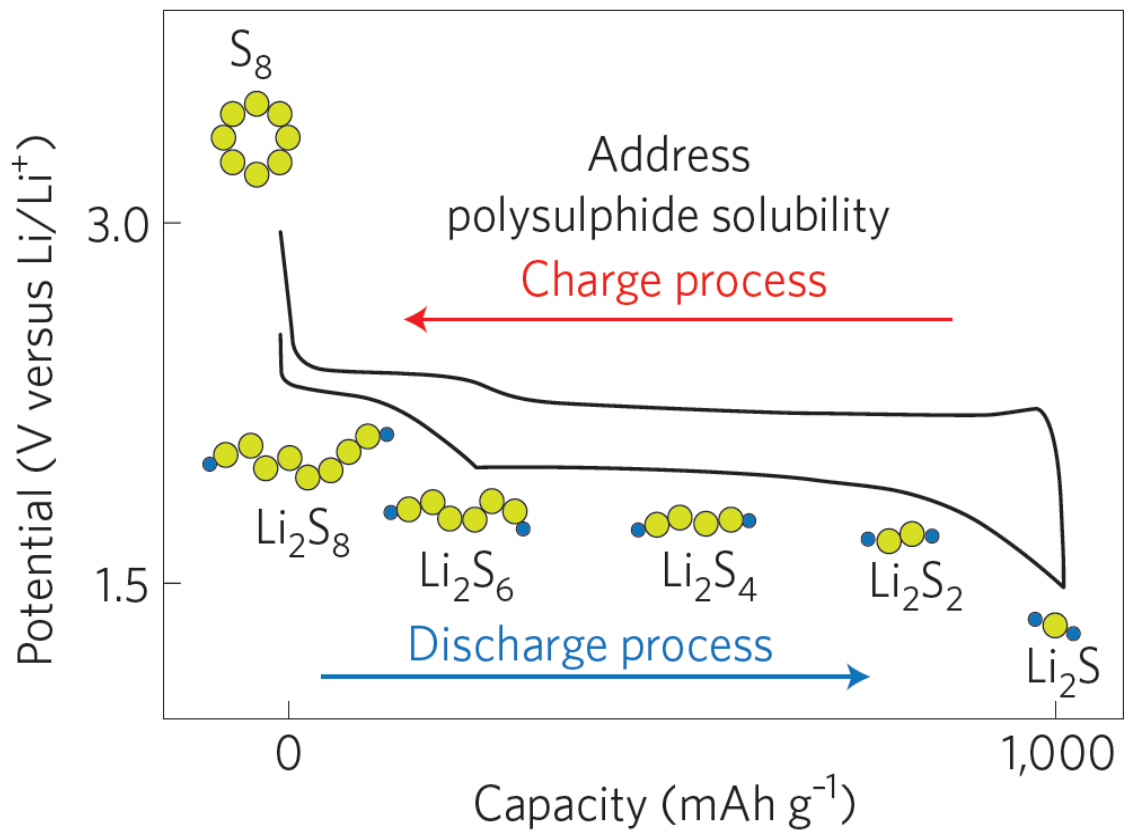


Figure 4. Representative charge/discharge curves for a lithium sulfur cell.

1.3. Research objectives.

In this chapter, we aim to provide a more detailed description of the intermediate product species formed in sulfur cathodes at various discharged and charged states, and an evidence for the migration of soluble lithium polysulfide toward Li metal anode by means of an air-tight Raman cell that we have developed. Additionally, we discuss the influence of ether-based solvents, which show different viscosity, on electrochemical reduction and oxidation of elemental sulfur on the basis of Raman studies. The discharge and charge capacities of Li-S cells with different electrolytes were also investigated.

2. Experimental

2.1. Preparation of lithium sulfur cell

For the electrochemical tests, A mixture of 70 wt% micrometer-sized elemental sulfur (100 mesh, Aldrich) and 20 wt% super P (as a carbon additive for conductivity enhancement, Timcal Inc.) was ball-milled for 5 min, and then a 10 wt% poly(vinylidene fluoride) (PVDF) ($M_w = 534,000$, Aldrich) binder in anhydrous *N*-methyl-2-pyrrolidinone (NMP, Aldrich) was added to the mixture. After mixing the cathode slurry, it was cast on a piece of aluminum foil (20 μm) by a doctor blade coating method and then dried in a convection oven at 80°C for 1 h. The thickness of all cathode films was about 28 μm and the sulfur loading was 0.7 mg cm^{-2} . The Li (600 μm) anode was prepared by laminating Li foil on a Cu current collector (18 μm) in a glove box. The electrolyte used was 1 M lithium bis(trifluoromethane sulfonyl)imide (LiTFSI) in three different solvents (tetra(ethylene glycol)dimethyl ether (TEGDME), 1,3-dioxolane (DOX), and their mixture) (received from Soulbrain Co.Ltd.)

2.2. Electrical properties measurements

Galvanostatic discharge and charge cycling (WonATech WBCS 3000 battery measurement system) was performed in the potential window from 1.5 to 2.8 V versus Li/Li⁺ with a two-electrode 2032 coin-type cell. The sulfur cathode electrode functioned as the working electrode and the Li metal foil as the counter electrode. In order to obtain a proper porosity, the sulfur cathode was not pressed and was spot-welded to the top of the coin cell. The first lithium insertion and extraction capacities were measured at a current density of 83.6 mA g^{-1} at 30.

2.3. Raman spectroscopy

A photo of an air-tight cell used in this work for Raman measurements is given in Fig. 5. After a coin-type cell was cycled, it was carefully opened in a glove box and a sulfur cathode retrieved from the disassembled cell was transferred to an air-tight cell. This airtight cell was assembled in a glove box filled with high purity argon gas. Sulfur cathodes and Li anodes for ex-situ Raman measurements were not washed, so that we could analyze all the species formed during discharging and charging. The Raman spectra were recorded at room temperature using an NRS-5100 micro Raman spectrophotometer (Jasco International Co., Ltd.), which was equipped with a single monochromator as a laser filter. Raman spectra were excited by a 532 nm laser.

2.4. X-ray diffraction (XRD)

X-ray diffraction (XRD) patterns of the cathodes before and after cycling were recorded using monochromatic Cu-K α radiation.

2.5. Focused Ion Beam (FIB) & Energy Dispersive Spectrometer (EDS)

The cross-sectional morphology of the sulfur cathode was obtained using a focused ion beam (Quanta 3D FEG) with a Ga source. During the acquisition of the images, an energy dispersive spectrometer (EDS) was also used to determine the types of chemical components in the region under investigation.

2.6. ^7Li NMR

Solid state ^7Li NMR experiments were performed on a Bruker DSX 400 MHz NMR spectrometer. The spin-lattice relaxation time (T_1) was determined using the spin-echo technique by applying 90° - τ - 90° pulse sequences.

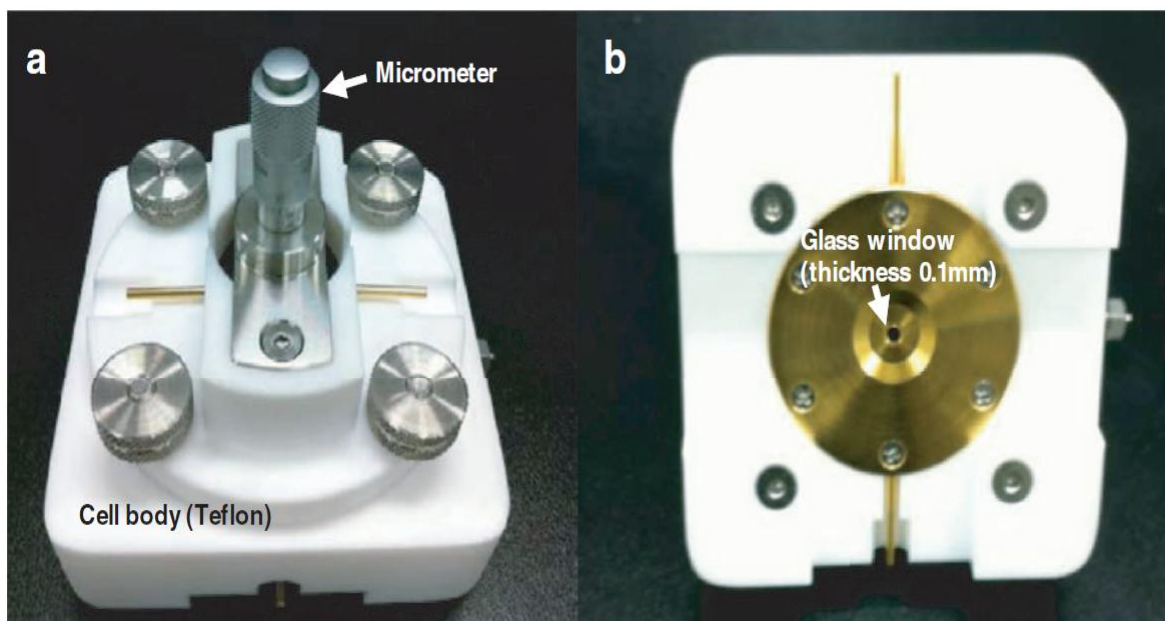


Figure 5. Picture of an air-tight cell for ex-situ Raman measurements. (a) Cell body. (b) Bottom of (a) with glass window that laser beam enters.

3. Results and Discussion

3.1. Images of sulfur cathodes

Cross-section images of sulfur cathodes are shown in Fig. 6a and 6c. It was found that the sulfur particle is fairly well covered by carbon black that is responsible for the electronic conduction and the carbon black layer contains poly(vinylidene fluoride) (PVDF) and sulfur phase dissolved from sulfur particle, as presented in Fig. 6a and 6b. It should be noted that a NMP solvent used for making electrodes partially dissolves sulfur particles. The inner part of sulfur particle consists entirely of elemental sulfur and has micropores. (Fig. 6c and 6d)

3.2 charge/discharge characteristics of lithium sulfur cell

Figure 7 shows the first discharge and charge profiles recorded at a current density of 83.6 mA g^{-1} during the first discharge. During discharge, sulfur is reduced to Li_2S_n ($n > 4$) at the upper potential plateau region (2.3 V vs. Li/Li^+); this Li_2S_n is further reduced to Li_2S_2 or Li_2S at the lower plateau region (2.1 V vs. Li/Li^+).²⁶ The initial discharge capacity of the cell with a mixed solvent of tetra(ethyleneglycol) dimethyl ether (TEGDME) and 1,3-dioxolane (DOX) (40/60, v/v) was 880 mAh g^{-1} , where the mass (g) refers to the sulfur active material. This value of 880 mAh g^{-1} is lower than the theoretical capacity of 1672 mAh g^{-1} . This discrepancy indicates that the complete reduction of sulfur active materials to Li_2S does not occur. To investigate the intermediate reaction species, seven different discharged and charged states (from a to g) were selected for the Raman spectral recording of sulfur cathodes, with results displayed in Fig. 7. Optical microscope images collected from each sulfur cathode without washing are presented in Fig. 8. A gray colored region formed by the long chain polysulfide (Li_2S_n , $n = 8$) and a non-reacted sulfur phase were observed after discharging to 2.28 V vs. Li/Li^+ . (Fig. 8b) After discharging to 1.5 V vs. Li/Li^+ , the gray colored region related to electrochemically generated lithium polysulfide mostly disappeared. During the charging process, bright regions, which may be attributed to lithium polysulfide, appear again and bright dots, shown in Fig. 8f, aggregated after full charging to 2.8 V vs. Li/Li^+ . The reason why the sulfur phase is exposed on the cathode surface is that the sulfur is formed by the lithium polysulfide diffusing away from the cathode side. From the optical microscope images, it can be seen that the electrochemical reduction and oxidation of sulfur cathode is reversible. Figure 9 presents the Raman spectra for sulfur cathodes for the various charged and discharged states shown in Fig. 7. The pristine cathode shows pronounced peaks corresponding to sulfur at 156, 221, and 473 cm^{-1} , as can be seen Fig. 9a.⁴⁶ The intensity of these peaks gradually decreased and peaks corresponding to intermediate polysulfide species (Li_2S_n , n

= 4 ~ 8) appeared during the discharge process. Raman results are in agreement with the previous reports.⁴⁷⁻⁴⁹ At a fully discharged state, no Raman peak corresponding to sulfur was detected and a peak attributed to the radical anion $S_3^{\cdot-}$ newly appeared (Fig. 9d). Previously, the $S_3^{\cdot-}$ species has been well identified by its Raman lines at 535 cm^{-1} .^{48,50} It was reported that the disproportionation equilibrium of S_4^{2-} could be a result of the reaction of $2S_4^{2-} \rightarrow 2S_3^{\cdot-} + S_2^{2-}$.⁴⁸ The presence of the $S_3^{\cdot-}$ species means that the disproportionation of Li_2S_4 forms the Li_2S_2 solid product, which can be electrochemically reduced to Li_2S . Even when an Li-S cell was discharged to 1.5 V vs. Li/Li^+ , there was no peak attributed to Li_2S (378 cm^{-1}). This is likely because the complete reduction of sulfur to insoluble Li_2S slightly occurs. The lower than theoretical capacity after the first discharge seems to be related to this result. During charging, peaks corresponding to elemental sulfur formed by the electrochemical oxidation of low order polysulfides (Li_2S_n , $n < 4$) were detected, as shown in Fig. 9f and 9g. From this result, the bright regions observed in the Raman images of Fig. 7f and 7g can be ascribed to sulfur phase in the cathode. The Raman image for point e in Fig. 7 has no bright regions. This is in agreement with the Raman results for point d, as shown in Fig. 9. Even after full discharge, Raman spectra did not show any evidence of Li_2S , as shown in Fig. 9d. The reason that the formation of insoluble Li_2S does not occur in a sulfur cathode can be explained from a following viewpoint. The reduction of insoluble Li_2S_2 to Li_2S , a diffusion-controlled reaction, is the most difficult due to the sluggishness of solid state diffusion of Li ions in the bulk (spin-lattice relaxation time (T_1) = 2044.06 s).⁹ Relatively high T_1 of Li_2S means that Li mobility in Li_2S is very low in comparison to LiTFSI (T_1 = 152.30 s). Poor contact of the low order polysulfide, Li_2S_2 , with the conductive carbon surface and the polysulfide dissolution problem may impede the formation of insoluble Li_2S , leading to a value of 50% of the theoretical capacity.^{23,51} The peak, which was not observed in the pristine sulfur cathode, is clearly seen around 746 cm^{-1} for the cathodes during the charge and discharge processes, and remains stable after full charging, as can be seen in Fig. 9g. This peak can be assigned to soluble lithium polysulfide (Li_2S_n , $4 \leq n \leq 8$) by the previous reports.⁴⁷⁻⁴⁹ The weak peak at 746 cm^{-1} , measured from the cathode at point g, means that the complete oxidation of polysulfide back to elemental sulfur does not occur and low order polysulfide coexists with elemental sulfur in a sulfur cathode.

In order to clarify the presence of Li_2S in the cathode, X-ray diffraction (XRD) patterns for fully discharged sulfur cathodes with and without washing were obtained. Comparing XRD patterns, as shown in Fig. 10, it can be observed that the elemental sulfur phase most likely disappears after the first discharge. This indicates that the crystalline elemental sulfur reacts with lithium ions and is converted to lithium sulfide by the electrochemical reduction. This is in good agreement with the previous results.⁵²⁻⁵⁵ In addition, the very weak and broad peak at only 26.98° arises from the Li_2S phase during discharge, while other peaks originating from Li_2S were not detected. This implies that

partially disordered Li_2S phase is formed by electrochemical reduction of Li_2S_2 during discharge. Recently, Cui group pointed out that crystalline Li_2S is not formed in in-situ XRD measurements and when a discharged cell is allowed to rest, crystalline Li_2S can be formed.⁵⁴ The Li_2S_2 or Li_2S solid phase precipitated on the cathode during the lower plateau region (2.1 V vs. Li/Li^+). The randomly precipitated Li_2S_2 or Li_2S (electronic conductivity = 3.6×10^{-7} S/cm by 4-point probe method) with insulating nature may block electron transfer toward the inside of the cathode and prevent the further reduction of high order polysulfides to Li_2S_2 or Li_2S . It is thought that poor electron transport of Li_2S_2 or Li_2S is one of limiting factors to hinder electrochemical reduction of polysulfide in the conventional composite sulfur cathode prepared by simply mixing bulk carbon and sulfur powder together. This is because electronic conducting pathway is not maintained in the conventional cathode during cycling. Therefore, intermediate products (soluble lithium polysulfides) largely exist during the discharge process in the cathode, as shown in Fig. 9d, and the difficulty of the reduction of polysulfide to Li_2S_2 or Li_2S results in low utilization of sulfur active materials (Fig. 7). It was reported that the trapping of the polysulfides within a sulfur cathode may promote the recrystallization of sulfur at the first charge cycle.⁵⁴ In contrast to previous report, the peak attributed to elemental sulfur was not recovered after full charge, as shown in Fig. 10e. It can be thought that the recrystallization of elemental sulfur does not readily occur at the first charge. Despite the absence of sulfur peak in the XRD pattern, the Raman results after full charge (Fig. 9g) manifest that elemental sulfur undergoes reversible electrochemical reactions at the first cycle.

Figure 11 presents Raman spectra of Li metal anodes retrieved from cells before and after cycling. It is clearly seen that lithium polysulfide species exist on a Li metal anode, as shown in Fig. 11b and 11c. This implies that lithium polysulfide formed in a sulfur cathode during discharge migrates toward Li anode.

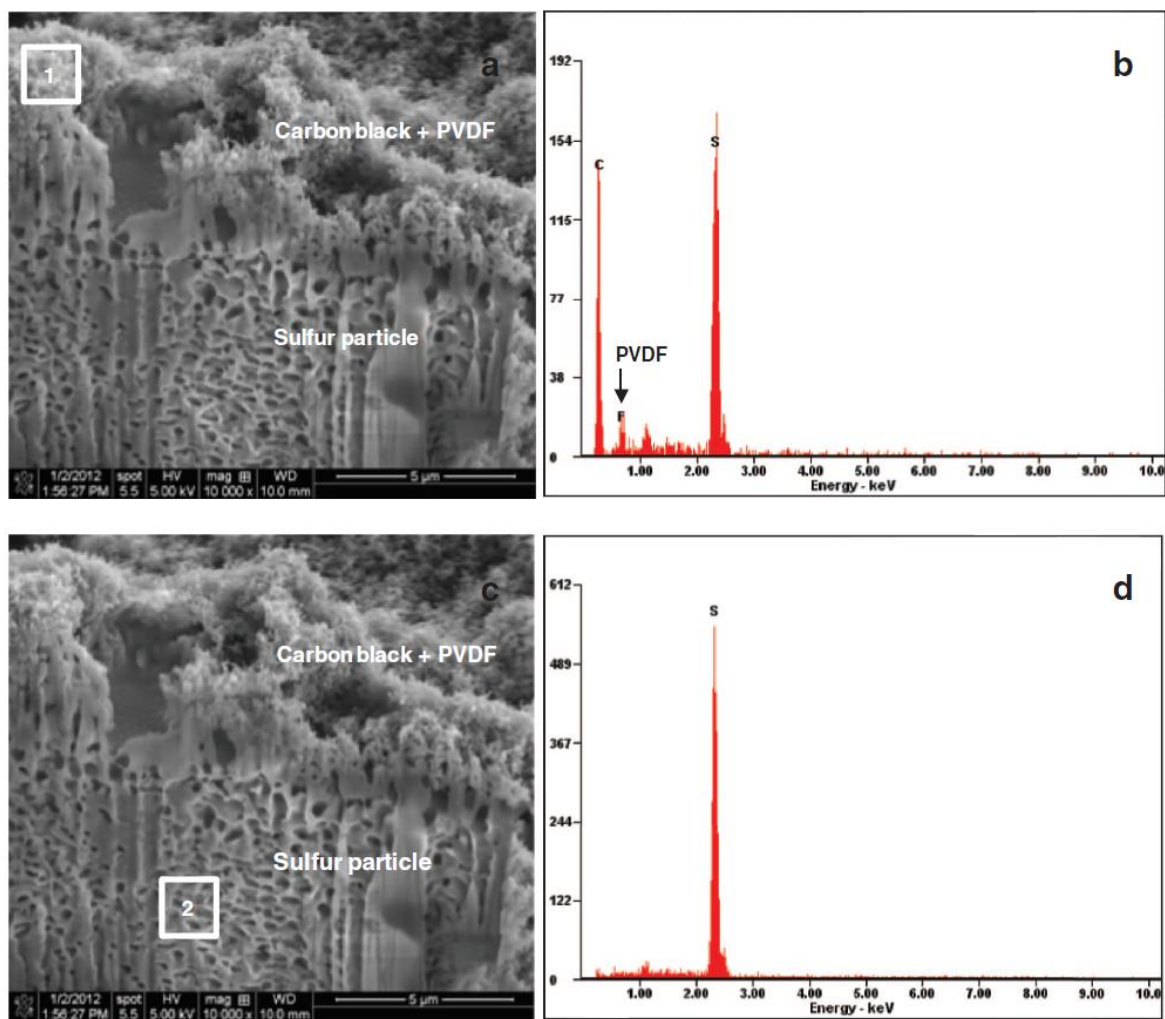


Figure 6. (a), (b) The cross-section images of sulfur composite cathodes and EDS spectra for (c) selected zone 1 and (d) selected zone 2.

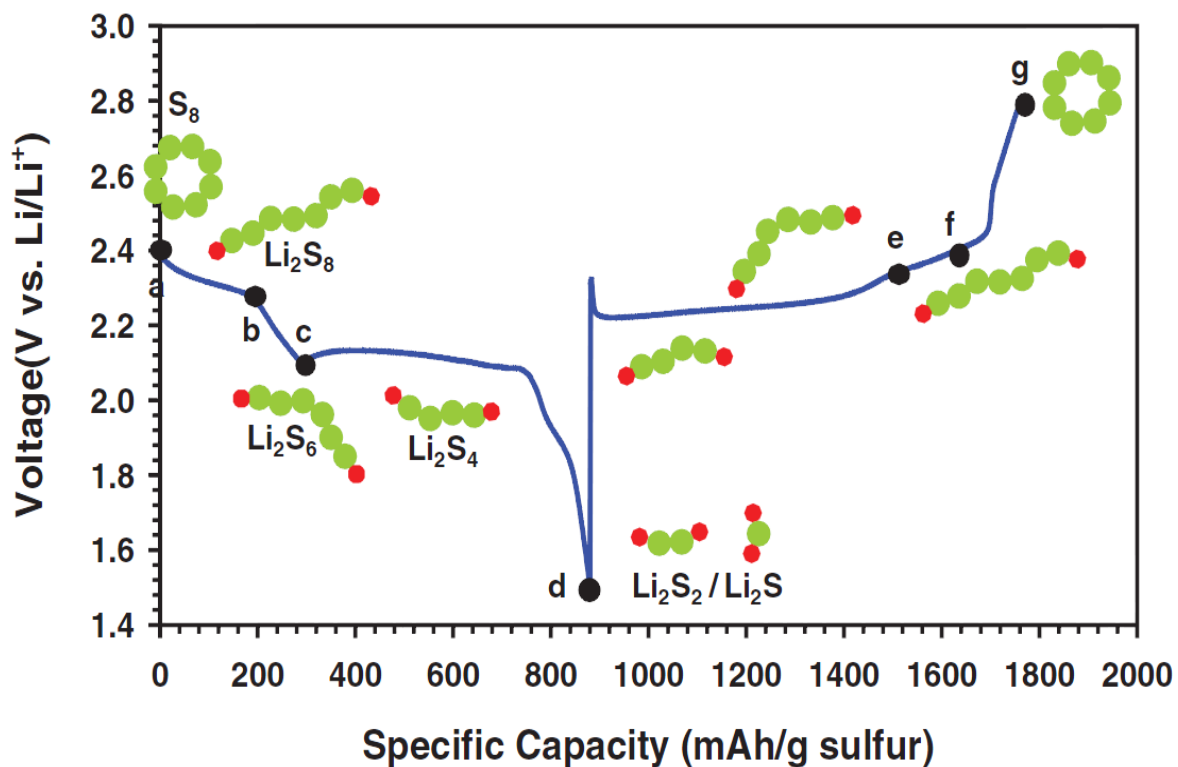


Figure 7. First discharge and charge profiles of a Li-S cell between 1.5 and 2.8 V vs. Li/Li⁺ at a current density of 83.6 mA g⁻¹ (C/20).

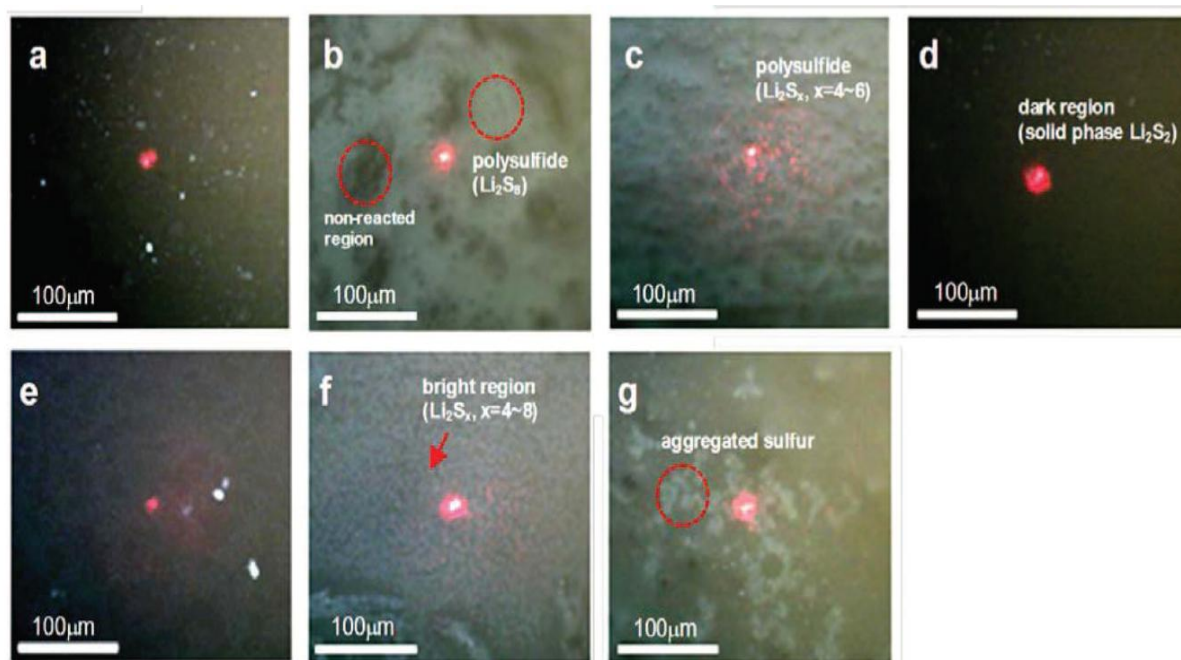


Figure 8. Optical microscope images showing the sulfur composite cathode surface at various discharged and charged states. (a) Pristine cathode. (b) Discharged to 2.28 V. (c) Discharged to 2.1 V. (d) Full discharge. (e) Charged to 2.34 V. (f) Charged to 2.4 V. (g) Full charge.

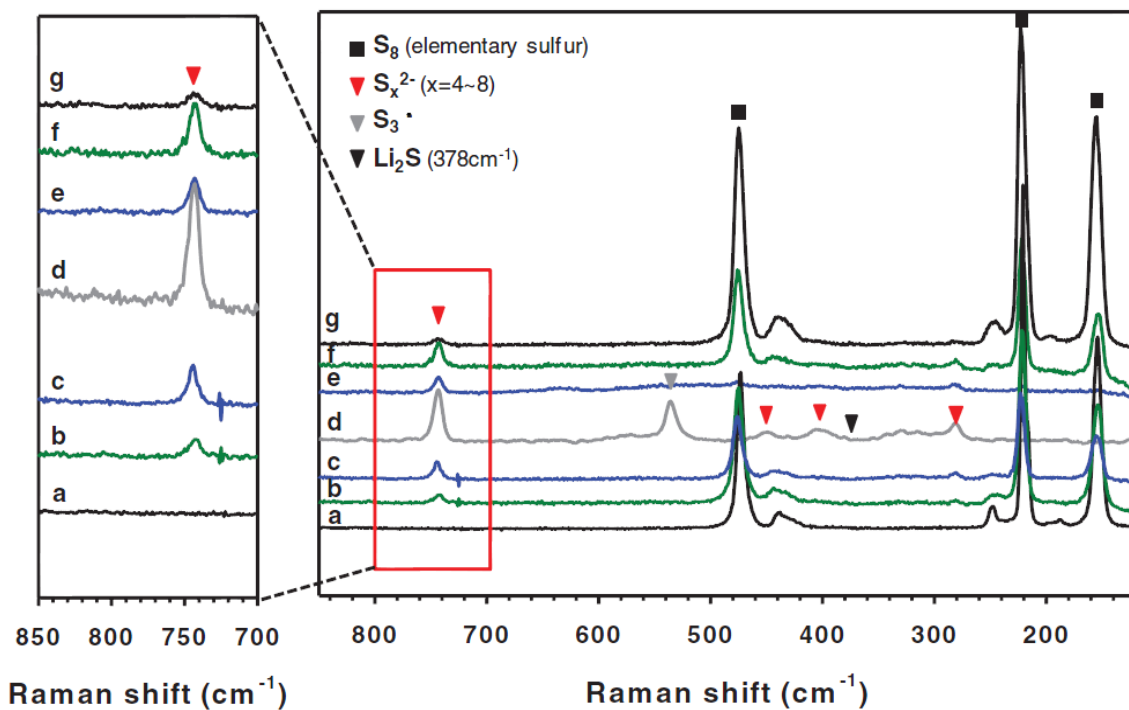


Figure 9. Raman spectra of sulfur cathodes obtained from seven representative points of Fig. 3. (a) Pristine cathode. (b) Discharged to 2.28 V. (c) Discharged to 2.1 V. (d) Full discharge. (e) Charged to 2.34 V. (f) Charged to 2.4 V. (g) Full charge.

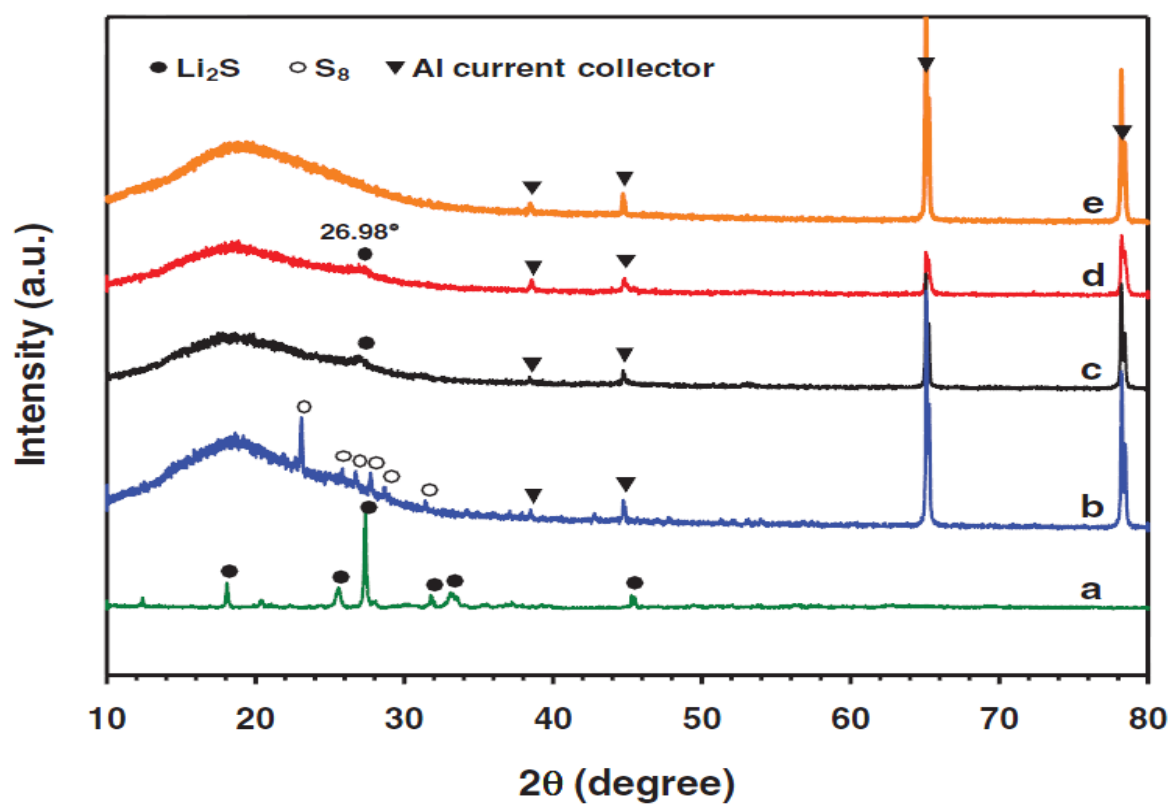


Figure 10. XRD patterns of the sulfur composite cathodes. (a) Li_2S powder. (b) Pristine sulfur cathode. (c) Fully discharged cathode without washing. (d) Fully discharged cathode with washing. (e) Fully charged cathode without washing.

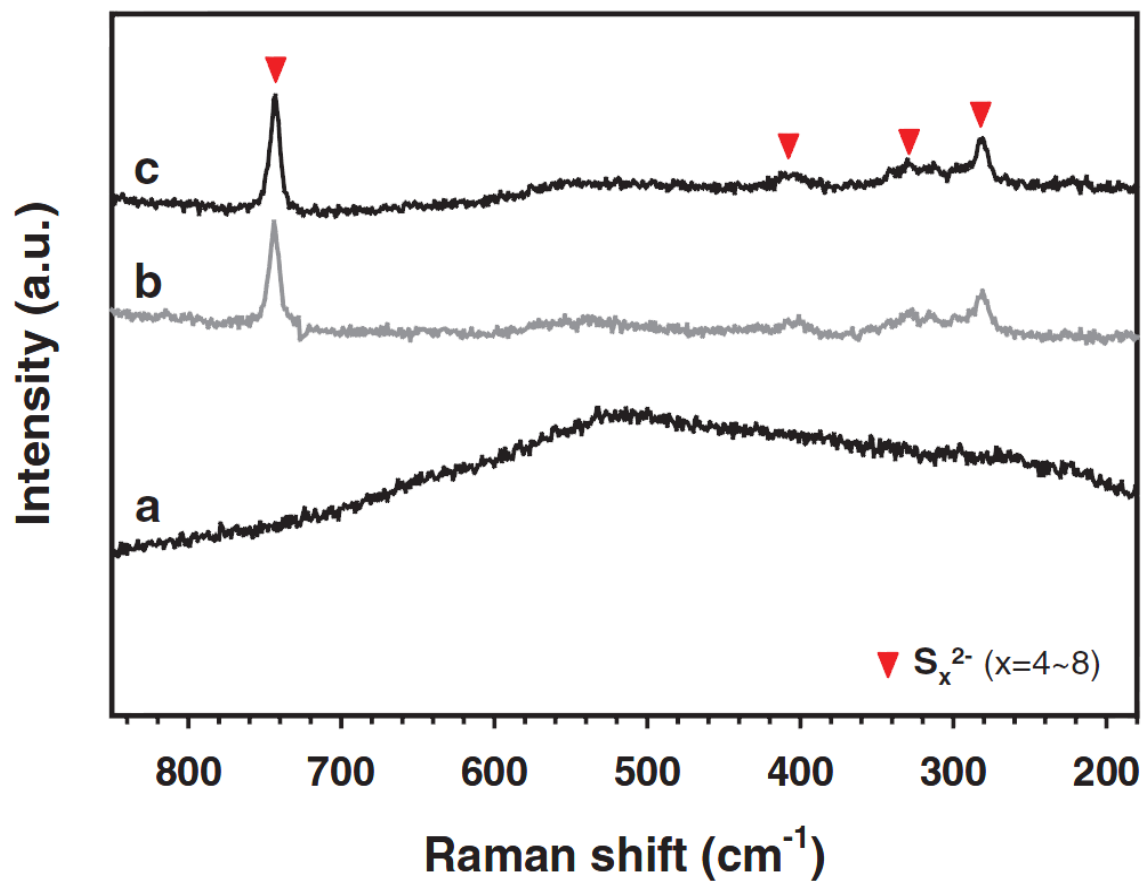


Figure 11. Raman spectra of Li metal anodes. (a) Before cycle. (b) After full discharge. (c) After full charge.

3.3 The effect of ether-based solvents on electrochemical performance

The effect of ether-based solvents on the discharge capacities of sulfur cathodes is shown in Fig. 12. The cells with TEGDME containing electrolytes were charged to 2.8 V vs. Li/Li⁺ without significant overcharge, while charging for the cell with a DOX-based electrolyte did not lead to an increase of the cell potential and led to considerable overcharging. It can be thought that DOX solvent does not effectively retard the polysulfide anion dissolution, which initiates the shuttle phenomenon. This is because of the low viscosity (0.6 cP at 25°C) of the DOX solvent. It is known that the diffusion rate of lithium polysulfide is closely linked to the medium viscosity.⁵⁶ The cell with the DOX-based electrolyte exhibited the lowest discharge capacity of 680 mAh g⁻¹, as shown in Fig. 12. In addition, the potential of the first plateau, which is associated with the reduction of elemental sulfur to soluble polysulfide (Li₂S₈), dropped, and the length of the first plateau, at which the elemental sulfur changes to soluble lithium polysulfide, decreased for the cell with the DOX-based electrolyte, as shown in Fig. 12. Poor dissolution of elemental sulfur (S₈(s)) in the DOX ($\epsilon \approx 7$)⁵⁷-based electrolyte may make electrochemical reduction of elemental sulfur to soluble lithium polysulfide difficult. At the higher potential plateau, the cells with TEGDME-containing electrolytes showed values of 209 mAh g⁻¹, which is 12.5% of the theoretical capacity (1672 mAh g⁻¹). This means that TEGDME based electrolytes facilitate the reduction of elemental sulfur to form soluble lithium polysulfide unlike DOX-based electrolyte. It should be noted that the dissolution ability of a TEGDME solvent ($\epsilon = 7.73$) toward the elemental sulfur is satisfactory to lead to electrochemical reduction of elemental sulfur at around 2.4 V.^{27,58} The cell with TEGDME/1M LiTFSI showed the highest discharge capacity of 1100 mAh g⁻¹. This is because the second plateau, at which the solid reduction products are formed, is profoundly dependent on the mixing ratio of TEGDME and DOX. First discharge curves show that the reduction of long chain lithium polysulfides to insoluble Li₂S₂ and Li₂S readily occurs in TEGDME-based electrolytes and contributes to the much higher discharge capacity.

Ex-situ Raman measurements for sulfur cathodes discharged and charged in different electrolytes were carried out to clarify the effect of TEGDME on the reduction of sulfur and the oxidation of lithium polysulfides. As seen in Fig. 13a and 13c, there was no indication of elemental sulfur when the sulfur cathodes were discharged in 1M LiTFSI dissolved in TEGDME or TEGDME/DOX. A possible explanation is that the elemental sulfur completely changes to lithium polysulfides during discharging. For the sulfur cathode discharged in TEGDME with 1M LiTFSI, the peak intensity corresponding to the radical anion S₃^{•-} was higher compared to that of TEGDME/DOX/1M LiTFSI and soluble lithium polysulfides were not detected. This result explains that the higher discharge capacity of Li-S cell with TEGDME/1M LiTFSI is closely linked to further reduction of Li₂S₂ produced by disproportionation of Li₂S₄, as illustrated in Fig. 14e. Even though the sulfur cathode was

fully discharged in DOX/1M LiTFSI, elemental sulfur remained. Another feature is the absence of a peak related to the radical anion $S_3^{\cdot-}$, as shown in Fig. 13e. After charging in 1M LiTFSI dissolved in TEGDME or TEGDME/DOX, peaks originating from elemental sulfur appeared due to the oxidation of lithium polysulfide, as shown in Fig. 13b and 13d. On the contrary, the sulfur cathode fully charged in DOX/1M LiTFSI displayed very low intensity of the peak attributed to elemental sulfur, as shown in Fig. 13f; lithium polysulfide were weakly detected, as shown in Fig. 13g. From this result, it can be stated that DOX/1M LiTFSI rarely allows the oxidation of lithium polysulfide to elemental sulfur.

Figure 14 shows ex-situ Raman images for sulfur cathodes discharged and charged in TEGDME or DOX-based electrolytes. For the fully discharged sulfur cathode in DOX/1M LiTFSI, a non-reacted sulfur region can be seen, as shown in Fig. 14a; a bright region, which is likely related to lithium polysulfide, can also be observed. Because of the lowered viscosity due to the relatively facile diffusion of the lithium polysulfide toward the bulk electrolyte, the outer layer of the cathode is a more likely site for the formation of the solid reduction products compared with the inside of the cathode, as depicted in Fig. 14e. Indeed, a noticeable layer is mostly formed not inside but the cathode surface, as shown in Fig. 14f and 14g. This is because soluble lithium polysulfide species formed by electrochemical reduction of elemental sulfur diffuse away from their original location in a cathode and insoluble Li_2S_2 and/or Li_2S products are precipitated on the cathode surface. On the other hand, the sulfur cathode discharged in TEGDME/1M LiTFSI showed no bright region. Importantly, in the case of the sulfur cathode charged in TEGDME/1MLiTFSI, the aggregated sulfur phase detected in Fig. 13b was clearly seen as aggregated form in Fig. 14d.

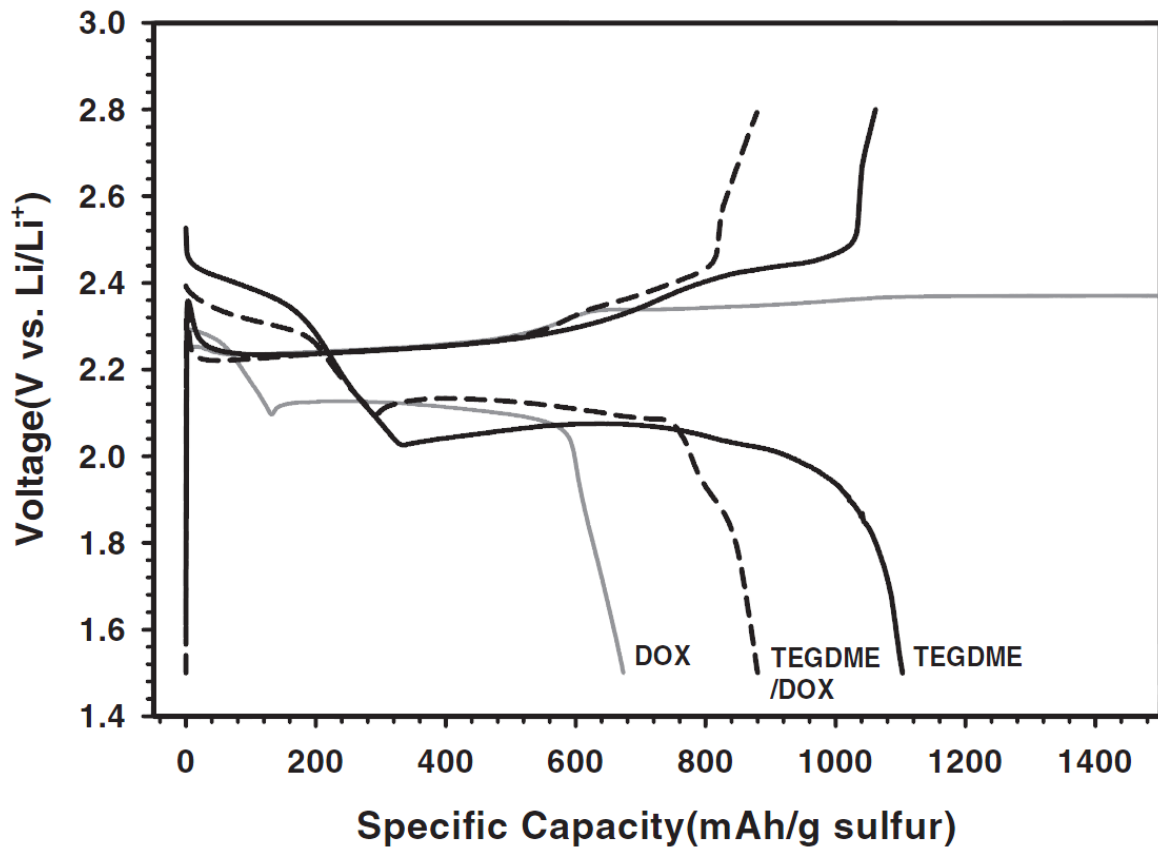


Figure 12. Comparison of discharge and charge profiles for a Li-S cell with a different electrolyte at a current density of 83.6 mA g^{-1} (C/20).

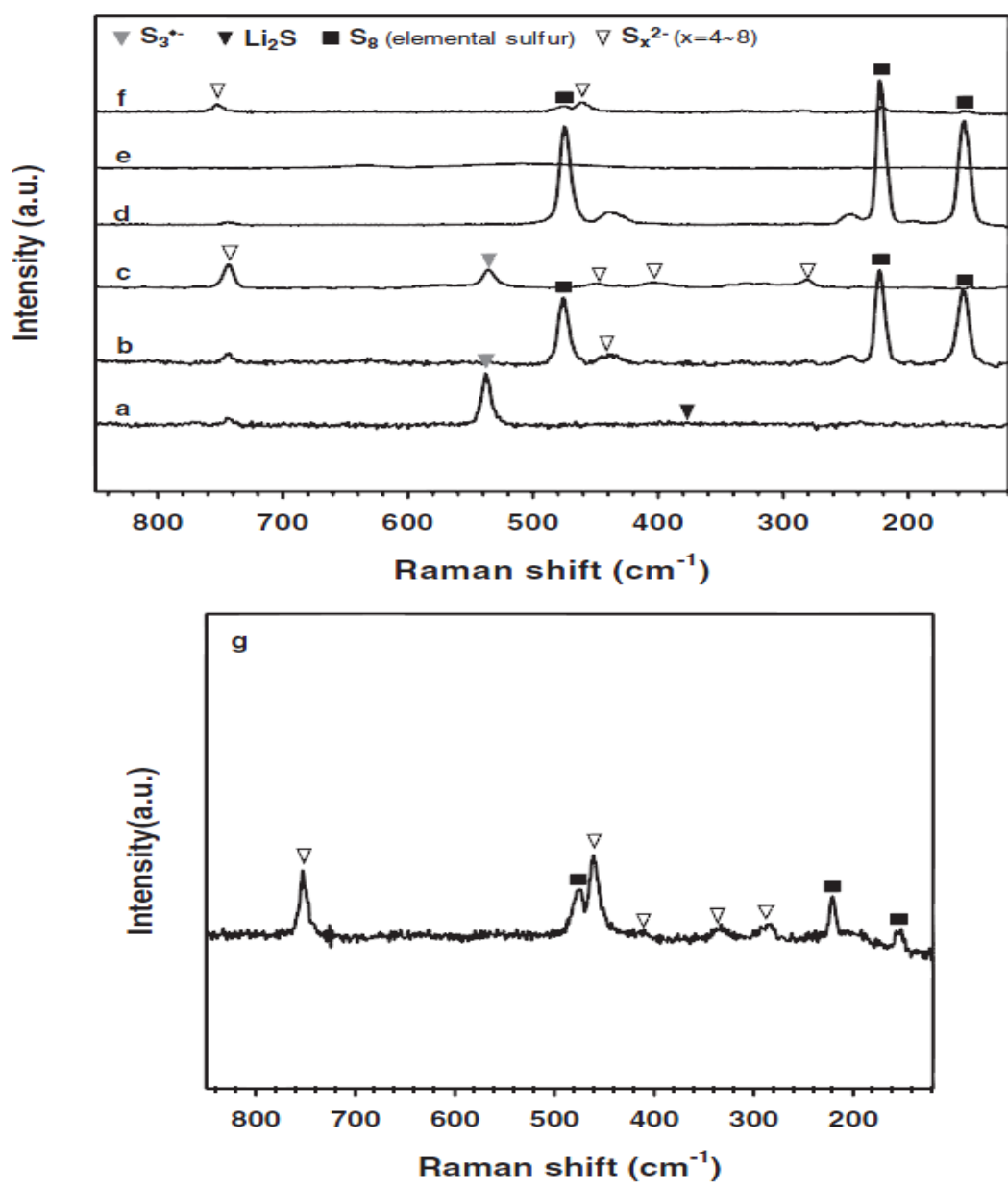


Figure 13. Raman spectra measured from the sulfur cathodes after (a) Fully discharged in TEGDME/1M LiTFSI. (b) Fully charged in TEGDME/1M LiTFSI. (c) Fully discharged in TEGDME/DOX (40/60) 1M LiTFSI. (d) Fully charged in TEGDME/DOX (40/60) 1M LiTFSI. (e) Fully discharged in DOX/1M LiTFSI. (f) Fully charged in DOX/1M LiTFSI. (g) Enlarged spectra of (f).

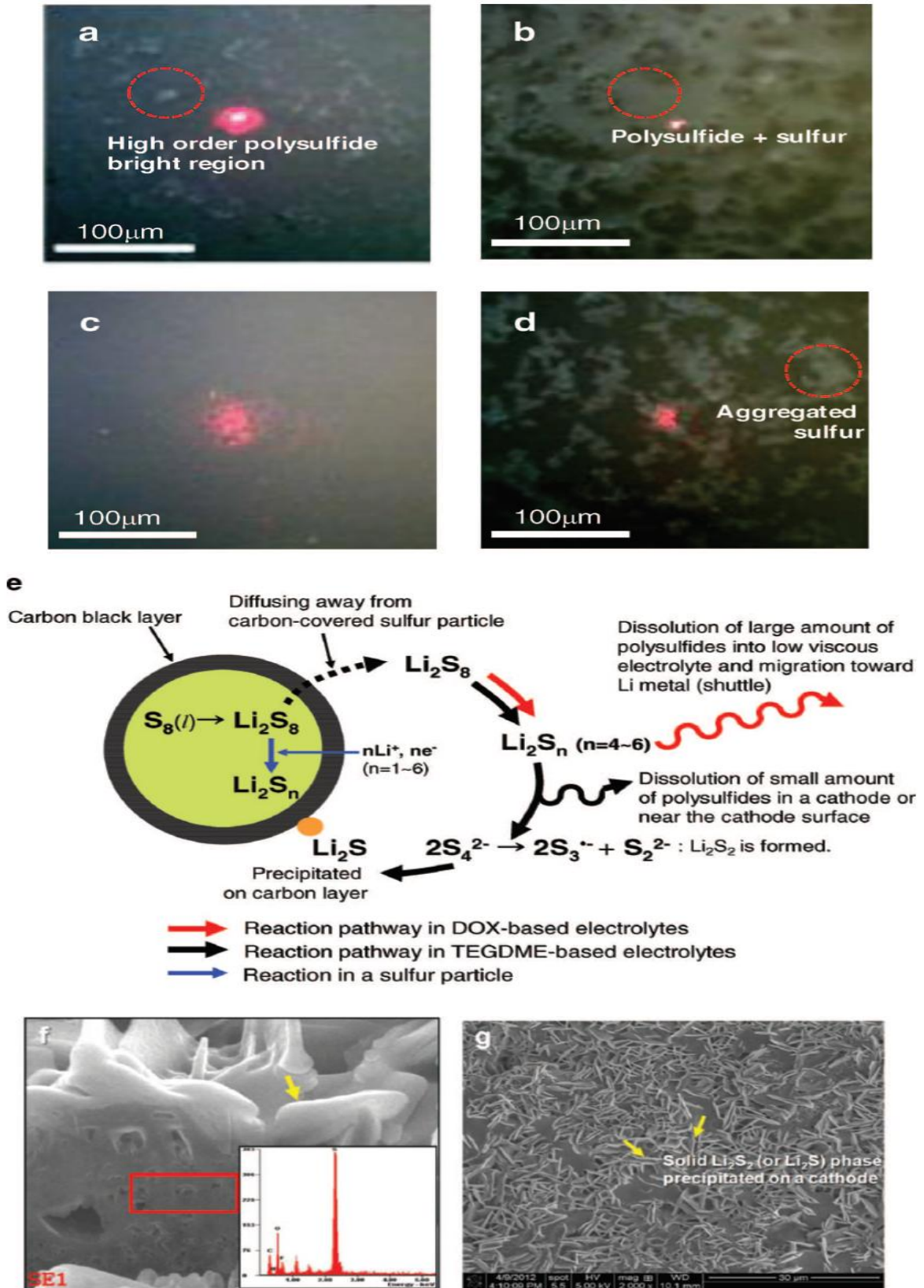


Figure 14. An optical microscope images showing the sulfur composite cathode surface after (a) Full

discharge in DOX/1M LiTFSI. (b) Charged up to 710 mAh g⁻¹ in DOX/1M LiTFSI (Compulsory capacity cutoff). (c) Full discharge in TEGDME/1M LiTFSI. (d) Full charge in TEGDME/1M LiTFSI. (e) Schematic drawing for reaction pathway in DOX- or TEGDME-based electrolytes. (f) SEM image of the cross section of a sulfur cathode fully discharged in TEGDME/DOX/1M LiTFSI with EDS spectrum. (g) SEM image of the cathode surface fully discharged in TEGDME/DOX (40/60) 1M LiTFSI.

4. Conclusions

Ex-situ Raman using an air-tight cell and XRD studies clearly confirmed that various lithium polysulfides, including the radical anion $S_3^{\cdot-}$ and partially disordered Li_2S , were formed at a fully discharged state, and elemental sulfur was fairly recovered after full charging in TEGDME/DOX/1M LiTFSI. Moreover, ex-situ Raman result clearly showed that soluble lithium polysulfide species migrate toward Li anode. Cycling tests and Raman results showed that DOX-based electrolytes prohibited the utilization of elemental sulfur and led to significant overcharge during the first charging process. The DOX-based electrolyte with low viscosity is strongly believed to cause a polysulfide shuttle during cycling. TEGDME-containing electrolytes could effectively mitigate overcharge and the dissolution problem of intermediate soluble polysulfide species during the first cycle.

CHAPTER III

Effect of fluoroethylene carbonate on electrochemical performances of lithium electrodes and lithium-sulfur batteries

1. Introduction

1.1. Rechargeable Lithium Anode

The motivation for using a battery technology based on Li metal as an anode relied initially on the fact that Li is the most electropositive (-3.04V versus standard hydrogen electrode) as well as the lightest (equivalent weight $M=6.94\text{g mol}^{-1}$, and specific gravity $\rho=0.53\text{ g cm}^{-3}$) metal, and a high specific capacity (3860mAh g^{-1}) thus facilitating the design of storage systems with high energy density. The advantage in using Li metal was first demonstrated in the 1970s with the assembly of primary Li cells.⁵⁹ Owing to their high capacity and variable discharge rate, they rapidly found applications as power sources for watches, calculators or for implantable medical devices. Thereafter, rechargeable lithium batteries based on Li metal were tried, but it encountered the shortcomings of a Li metal/liquid electrolyte combination - uneven (dendritic) Li growth as the metal was replated during each subsequent discharge-recharge cycle, which led to explosion hazards. This poor safety hindered them to be commercialized. To circumvent the safety issues surrounding the use of Li metal, several alternative approaches were pursued in which either the electrolyte or the negative electrode was modified. The first approach involved substituting metallic Li for a second insertion material. The concept was first demonstrated in the laboratory by Murphy et al.⁶⁰ and then Scrosati et al.⁶¹ and led, at the end of 1980s and early 1990s, to the so-called Li-ion or rocking-chair technology. Li ion batteries consisting of C/LiCoO₂ electrodes came to a market as a rechargeable lithium battery. The second approach involved replacing the liquid electrolyte by a dry polymer electrolyte, leading to the so-called Li solid polymer electrolyte (Li-SPE) batteries.⁶² But this technology is restricted to large systems (electric transportation or backup power) and not to portable devices, as it requires temperatures up to 80°C. Shortly after this, several groups tried to develop a Li hybrid polymer electrolyte (Li-HPE) battery, hoping to benefit from the advantages of polymer electrolyte technology without the hazards associated with the use of Li metal.⁶³ 'Hybrid' meant that the electrolyte included three components: a polymer matrix swollen with liquid solvent and a salt.

1.2. Intrinsic Properties of Lithium Metal Electrode and Approaches for its Stabilization

In general, the surface of metallic lithium electrode is covered with a “native layer” consisting of various lithium compounds such as LiOH, Li₂O, Li₃N, Li₂CO₃. These compounds are produced by the reaction of lithium with O₂, H₂O, CO₂ or N₂. These compounds can be detected by X-ray photoelectron spectroscopy (XPS). Inner layer and outer layer of a native layer mainly consist of Li₂O and LiOH /Li₂CO₃, respectively.

The chemical or electrochemical reactivity of lithium electrode with electrolyte solution leads to a formation of SEI (solid electrolyte interphase) layer. The SEI layer, which contains the products of reactions between lithium and the plasticizer, salt, and their impurities, is composed of various organic and inorganic compounds as shown in Fig. 15. The structure of SEI layer changes more complex morphology with the repeated cycling. It acts as an interphase between the lithium electrode and the organic electrolyte. In addition, the formation of lithium dendrite by the non-uniform current distribution on the lithium electrode surface can result in the unexpected behaviors such as capacity loss, low cycling efficiency, poor cycleability, and explosion hazards as shown in Fig. 16 [Tatsuma *et al*, 1999; Naoi *et al*, 1999]. Therefore, it is quite important to control the lithium electrode/polymer electrolyte interface to obtain the higher energy density and the good cycling efficiency of lithium rechargeable batteries. It is generally accepted that the electrochemical properties of the metallic lithium electrode depend mostly on the nature of the electrolyte. In most of the electrochemical systems with a lithium electrode, the formation of a SEI layer is observed at the interface between the metallic lithium and liquid electrolyte or polymer electrolyte. The rate-determining step for the lithium charge transfer reaction is associated with the ionic transport properties in the SEI layer. The charge transfer reaction is limited by the surface coverage of the lithium electrode. Whatever the nature and morphology of SEI layer, its presence modulates the performance of the lithium electrode, generally reducing the rechargeability [Zhuang *et al*, 2000; Tirado *et al*, 2003]. This is caused by a decrease in the active surface area and/ or increase in the diffusion resistance of the lithium ions in the passivation layer. Lithium deposition and dissolution occur through an interphase formed on the lithium electrode due to reductive reaction of the electrolyte components such as plasticizer, salt anion, and impurities. When these processes are not uniform, Li deposition is very dendritic, causing a gradual loss of the anode material upon charge-discharge cycling. In recent, it was reported that the modification of the lithium electrode surface affects lithium cycling efficiency. Much effort has been exerted to improve the surface uniformity of the SEI layer and to form electrochemically stable SEI layer through the modification of lithium metal as shown in Figure 17. The modifications of lithium metal can be divided into :

- Chemical modifications

- Formation of Li₂CO₃, LiF, LiOH, or polysulfide : CO₂, HF, water trace, S_x²⁻

- Formation of metal alloy : SnI, AlI₃
- Surfactant : non-ionic polyether
- Physical modifications
 - Pressure, Temperature
 - Inorganic filler : silica, alumina, zeolite, titanate
 - Ultra-thin polymer layer by plasma polymerization: Fluoropolymer

The formation of passivation layer on the lithium surface is promoted by adding agents such as CO₂ [Aurbach *et al.*, 1994; Osaka *et al.*, 1995;1999], HF [Kanamura *et al.*, 1994; Shiraishi *et al.*, 1999], or S_x²⁻ [Besenhard *et al.*, 1993; Wagner *et al.*, 1997] and thus the dendritic lithium formation can be much suppressed. SnI and AlI₃ were also proposed as additives to improve the lithium rechargeability [Ishikawa *et al.*, 1994, 1999]. Both Sn and Al are well known to form lithium alloys [Matsuda *et al.*, 1993]. It is supposed that the thin layers of the lithium alloys at the electrode surface during the deposition the dendritic deposition of lithium, which causes the lowering of the coulombic efficiency. When the polyether surfactant such as poly(ethylene glycol)dimethyl ether (PEGDME) was used as a additive, significant suppression of the inactivation of deposited lithium was reported [Naoi *et al.*, 2000]. Crucial effect of physical factors such as temperature and pressure on the improvement of the lithium cycling performance was reported [Hirai *et al.*, 1994; Ishikawa *et al.*, 1999]. The addition of inorganic fillers could enhance the interfacial stability to lithium electrode due to the trap capability for liquid impurities [Kumar *et al.*, 1994; Slane *et al.*, 1995; Croce *et al.*, 1998; Appetecchi *et al.*, 2000]. Another approach for controlling the passivation layer formation has been taken by forming an ultra-thin plasma polymer layer of the solid polymer electrolyte on the lithium anode surface [Takehara *et al.*, 1993]. To protect the reactive lithium metals by covering their surface with organic compound would be one of the smart ways to minimize the passivation and the dendritic growth of lithium on lithium metal surface.

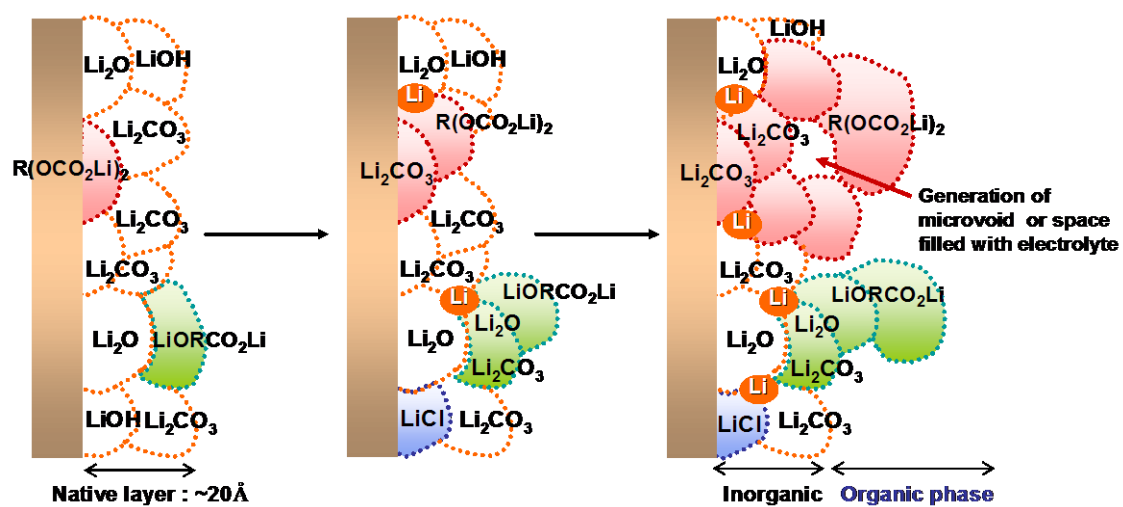


Figure 15. Schematic illustration for the formation and growth of SEI layer on the lithium electrode.

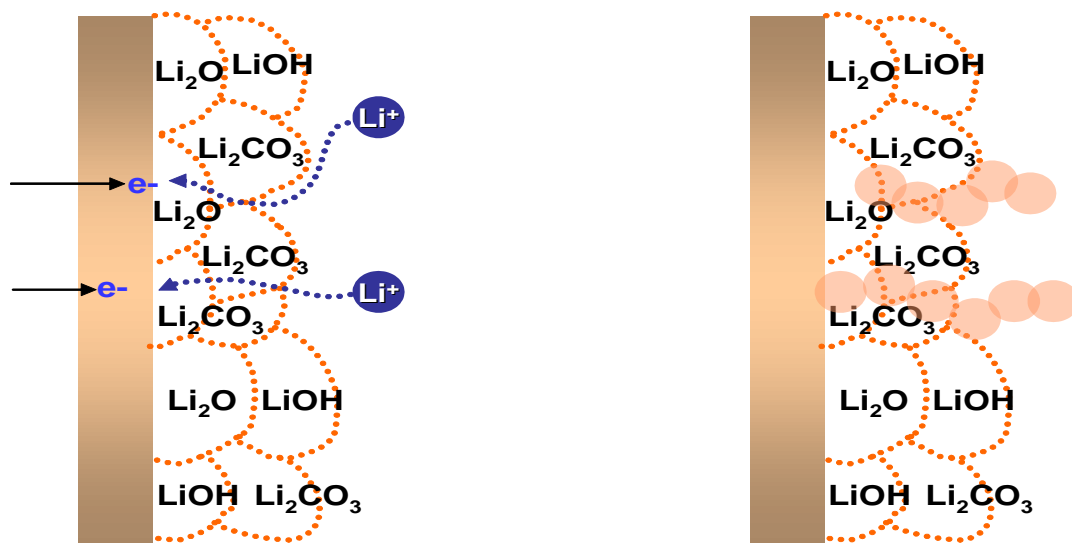


Figure 16. Schematic illustration for the formation of dendritic lithium on the lithium electrode.

Year	1990	1995	1999	2000
Polymer electrolyte	Plazama-polymerized thin layer based on PVdF/LiClO ₄			
Physical factor		Pressure	Pre-cycling at low temperature	
Control of SEI layer properties		Inorganic filler		
		HF		
		N ₂ O, S _x ²⁻		
		H ₂ O, CO ₂		
		SnI ₂ /AlI ₃		
Surfactant				PEGDME
				Fluorinated salt surfactant

Figure 17. Modification history for stabilization of the lithium metal electrode

1.3. Lithium metal electrode/ electrolyte interface

It is generally accepted that in polymer electrolyte systems, the lithium electrode is covered by a “resistive layer” [Fauteux *et al.*, 1993; Peled *et al.*, 1995]. This layer plays a major role in determining their properties, which include shelf life, safety, lithium deposition/dissolution efficiency and cycle life. The interphase models have been developed for compositions which result in surface layers with properties of a solid electrolyte and are as follows.

1.3.1. SEI model I : Homogeneous layers

1.3.1.1. Solid Electrolyte Interphase (SEI) model

The equivalent circuit and impedance diagram for the conducting process in the SEI layer are shown in Fig.18(a). This circuit consists of the bulk resistance, R_b and the geometric capacitance, C_g which are related to the conductivity, and the permittivity, as follows ; $R_b = Y/\sigma$, $C_g = \epsilon/Y$

Where Y is the thickness of the solid electrolyte. The corresponding impedance diagram in the complex plane consists of a semicircle due to the R_b/C_g coupling over the whole frequency range. By analyzing this diagram one can determine the thickness of the surface layer for a known permittivity or conductivity of the solid electrolyte.

1.3.1.2. Polymer Electrolyte Interphase (PEI) model

The equivalent circuit and impedance diagram related to the PEI layer are given in Fig.18(b) for a case where the elementary processes can be separated. The equivalent circuit is determined by three types of impedances : (i) conduction impedance defined by the bulk resistance and the geometric resistance and the double layer capacitance; (ii) charge transfer impedance represented by the charge transfer; (iii) diffusion impedance determined by a finite thickness of the diffusion layer.

1.3.2. SEI model II : Composite and Stratified layers

1.3.2.1. Solid Polymer Layer (SPL) model

In this model, the surface layer is assumed to consist of solid compounds dispersed in a polymer electrolyte. As shown in Fig.18(c), the equivalent circuit of the lithium covered by such a solid polymer interphase can be similar to that of the PEI model. In the SPL case, the different time

constants of the conduction, charge transfer, and diffusion processes may not be well separated. The three loops then mix to form a single distorted loop, which can only suggest the existence of the several processes.

1.3.2.2. Compact Stratified Layer (CSL) model

In this model, the surface layer is assumed to be made of two layers as shown in Fig.18(d). The first sublayer is a solid electrolyte on the electrode surface, and the second layer is either a solid or a polymer electrolyte. These sublayers have different permittivities and conductivities. The equivalent circuit consists of the circuit of a SEI layer in series with the circuit of a SEI or a PEI layer.

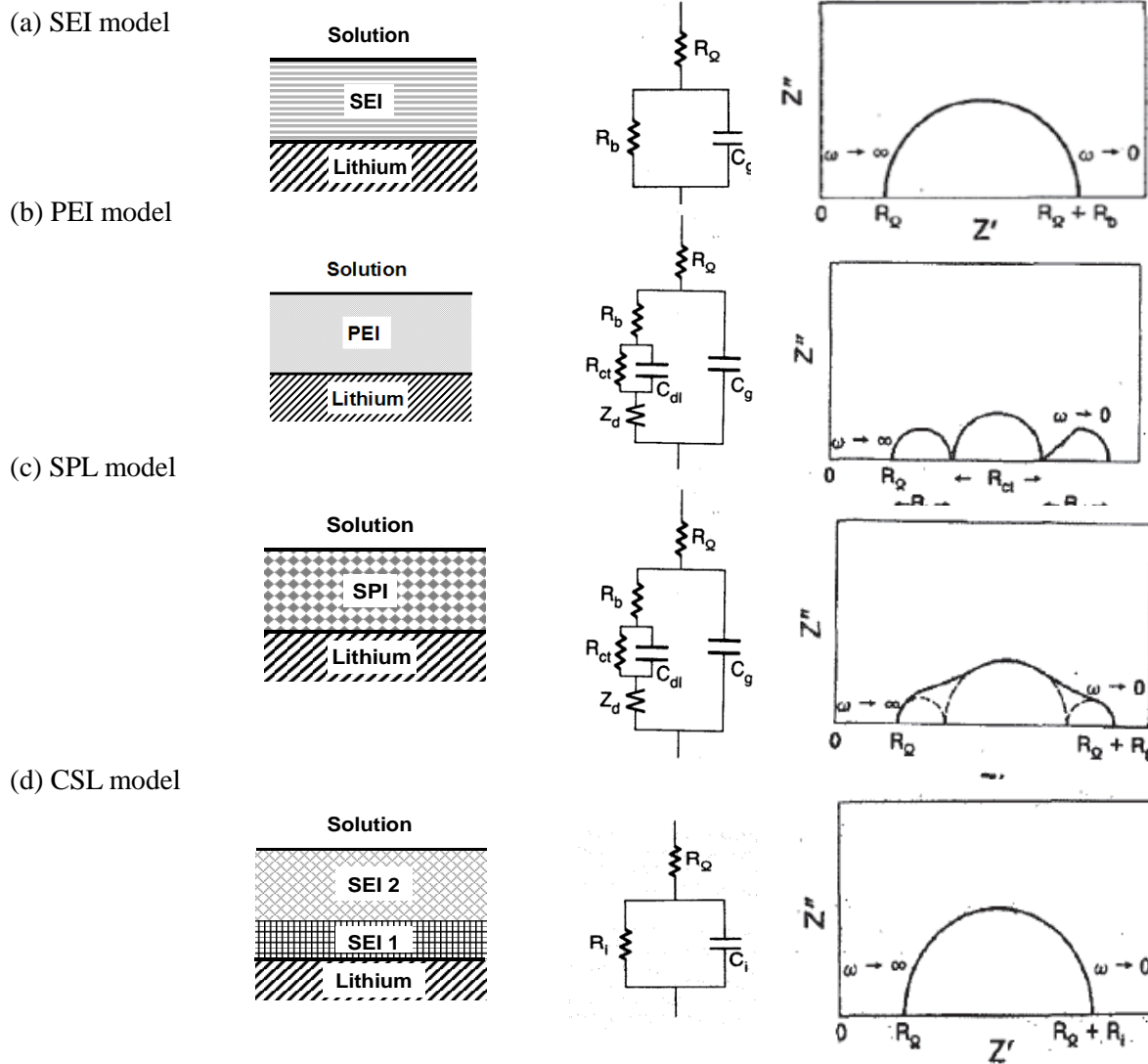


Figure 18. Different interphase model of the lithium electrode/organic electrolyte Interface

1.4. Protection layer on Li metal

For Li-S batteries, lithium metal is used as the anode, i.e. as the lithium source to provide a high energy density. However, lithium is so reactive that it usually results in poor charge/discharge cycling efficiencies due to severe growth of the SEI layer.^{23,24,64,65} In addition, dendrite formation on the Li electrode during the Li deposition, which can cause short-circuits, and undesirable reaction of the Li electrode with the electrolyte solution should be overcome. For this reason, modification of the surface of the Li anode has been previously studied. For instance, Ogumi and co-workers^{66,67} generated the protection layer on the Li anode by plasma polymerization, and Osaka et al.^{68,69} induced the formation of a Li_2CO_3 layer on the surface of the Li anode by exposing the electrode to carbon dioxide. PolyPlus Co.⁷⁰ presented research on glass electrolytes sputtered on the Li anode and applied them to Li-S batteries. It was also reported that the inclusion of a protective film based on a crosslinked gel polymer electrolyte is an effective means of mitigating undesirable reactivity of the Li electrode.⁷¹⁻⁷³ Though a significant overcharge of Li-S battery was suppressed by the introduction of the protection layer, its discharge capacity was lower than that of the nonprotected Li/S cell.⁷⁴ This is likely due to the fact that the protection layer with tetra(ethylene glycol) dimethyl ether (TEGDME), acts as a resistive layer.

1.5. Research objectives

In this chapter, we report the effect of FEC on the dissolution and deposition of Li metal during galvanostatic cycling of lithium symmetrical cells. . In order to retard the movement of soluble polysulfides toward an Li electrode and stabilize the Li metal electrode more effectively,⁷⁵⁻⁸¹ the protective polymer film physically separated with bulk electrolyte is formed on the Li electrode of a Li-S cell. The protection layer on the Li anode was newly prepared by a UV cured polymerization method. To the best of our knowledge, we first demonstrate the significant role of a polymer thin film with FEC in electrochemical performances of Li-S batteries.

2. Experimental

2.1. Preparation of lithium sulfur cell

For the electrochemical tests, a mixture of 70 wt% micrometer-sized elemental sulfur (100 mesh, Aldrich) and 20 wt% super P (as a carbon additive for conductivity enhancement, Timcal Inc.) was ball-milled for 5 min, and then a 10 wt% poly(vinylidene fluoride) (PVDF) ($M_w = 534,000$, Aldrich) binder in anhydrous *N*-methyl-2-pyrrolidinone (NMP, Aldrich) was added to the mixture. After mixing the cathode slurry, it was cast on a piece of aluminum foil (20 μm) and then dried in a convection oven at 80 °C for 1 h. The thickness of all cathode films was about 28 μm and the sulfur loading was 0.7 mg cm^{-2} . The bulk electrolyte used for electrochemical tests of Li-S cells was 1.0 M lithium hexafluorophosphate (LiPF_6) in tetra(ethylene glycol) dimethyl ether (TEGDME) (received from Soulbrain Co. Ltd.). Ethylene carbonate (EC)/ethylmethyl carbonate (EMC) (30/70, v/v) and fluoroethylene carbonate (FEC) were mixed at various volume ratios and a 1 M concentration of LiPF_6 was dissolved in the resulting mixed solvent. The composition of each electrolyte is listed in Table 2.

Table 2. Composition of various electrolytes

Electrolyte	EC/EMC ^a	FEC ^b	TEGDME ^c	Li salt
	vol%			
Ref	100			1M LiPF_6
FEC60	40	60		1M LiPF_6
TEGDME			100	1M LiPF_6

a A volume ratio of EC and EMC = 30 : 70.

b and c are fluoroethylene carbonate and tetra(ethyleneglycol) dimethyl ether, respectively.

2.2. Electrical properties measurements

2.2.1. Li-Li symmetrical cell

For electrochemical tests of Li symmetrical cells, a coin-type half cell (2016) with a lithium working electrode and a Li metal electrode used as a counter electrode was assembled in an argon filled glove box with less than 1 ppm of both oxygen and moisture. Cycling experiments for Li symmetrical cells were galvanostatically performed at a rate of C/10 using a computer-controlled battery measurement system (WonATech WBCS 3000).

2.2.2. Lithium sulfur cell

Galvanostatic discharge and charge cycling of Li-S cells were performed in a potential window from 1.5 to 2.8 V versus Li/Li⁺ with a two-electrode 2032 coin-type cell at 30°C. The sulfur cathode electrode functioned as the working electrode and the Li metal foil as the counter electrode. Microporous polyethylene film was used as a separator. Cells were assembled in an Ar-filled glove box with less than 1 ppm of both oxygen and moisture. In order to obtain proper porosity, the sulfur cathode was not pressed and was spot-welded to the top of the coin cell. The first lithium insertion and extraction capacities were measured at a current density of 83.6 mA g⁻¹ (C/20 rate) and further cycling was carried out at a current density of 167.2 mA g⁻¹ (C/10 rate).

2.3. Characterization of Li metal after dissolution & deposition

The surface morphology of the Li electrode was observed by means of a field emission scanning electron microscope (FE-SEM; JEOL JSM-6700F). During the acquisition of the SEM image, an energy dispersive spectrometer (EDS) was also used to determine the kind of chemical components in the region under investigation. Attenuated total reflectance–Fourier transform infrared (ATR-FTIR) spectra of the Li electrode surface after the Li dissolution were recorded in reflectance measurements using a Varian 670-IR spectrometer with a spectral resolution of 4 cm⁻¹ under a nitrogen atmosphere. Time of flight secondary ion mass spectrometry (ToF-SIMS) measurements were performed using a spectrometer (ION TOF, Germany) at a dose density of 2.25 x 10¹³ ions cm⁻² and an analysis area of 50 x 50 μm². The pressure in the chamber was maintained below 1.0 x 10⁻⁶ Pa. The ion maps were recorded by using a 25 keV Bi⁺ ion source. The characteristics of the interface between the electrolyte and the lithium electrode were examined by monitoring the impedance of Li/ electrolyte/Li cells.

2.4. Preparation of lithium and protected lithium anodes

A protective layer based on a semi-interpenetrating polymer network (IPN) structure was generated on the lithium electrode surface by UV-curing polymerization. The UV-curable formulation consists of a curable monomer (1,4-butanediol diacrylate, Aldrich), a P(VdF-co-HFP) ($M_w = \sim 400,000$, Aldrich) dissolved in purified tetrahydrofuran, FEC/1M LiTFSI, and a photoinitiator (benzophenone, 3wt% based on curable monomer). A curable mixed solution was coated on the lithium metal surface, and after 10 min of drying, it was irradiated with UV light for 3 min. The protective layer based on a semi-IPN structure was then formed on the lithium electrode^{71,72}, as depicted in Fig. 19(a); its composition is summarized in Table 3. The SEM image of the protection layer formed on the Li electrode is shown in Fig. 19(b). The unit cells were fabricated by sandwiching the polyethylene separator containing a liquid electrolyte between the sulfur cathode and the metallic lithium anode protected with a gel polymer electrolyte, as shown in Fig. 19(c).

Table 3. Composition of protection layers formed on the Li electrode surface in Li-S cells

	TEGDME	FEC60	1,4-butanediol diacrylate	P(VdF-co-HFP)
	wt%			
Protection layer 1	60		20	20
Protection layer 2		60	20	20

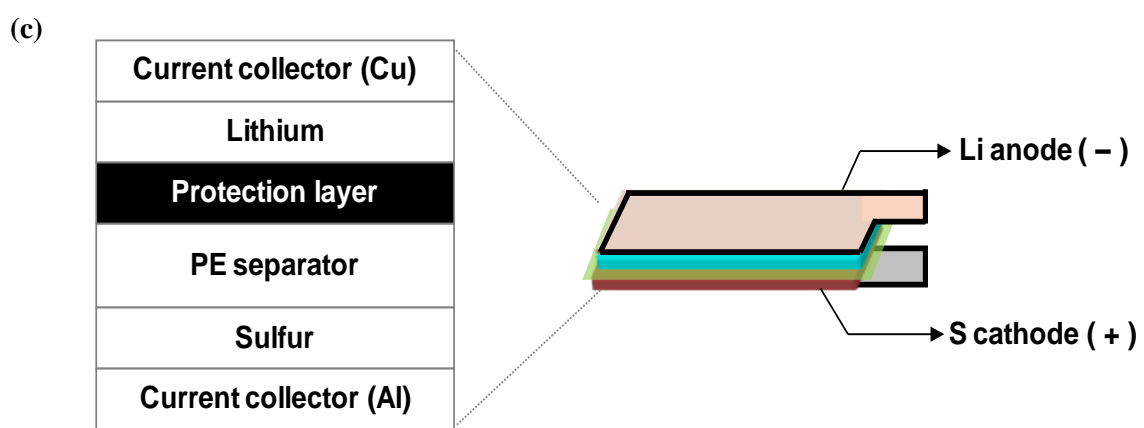
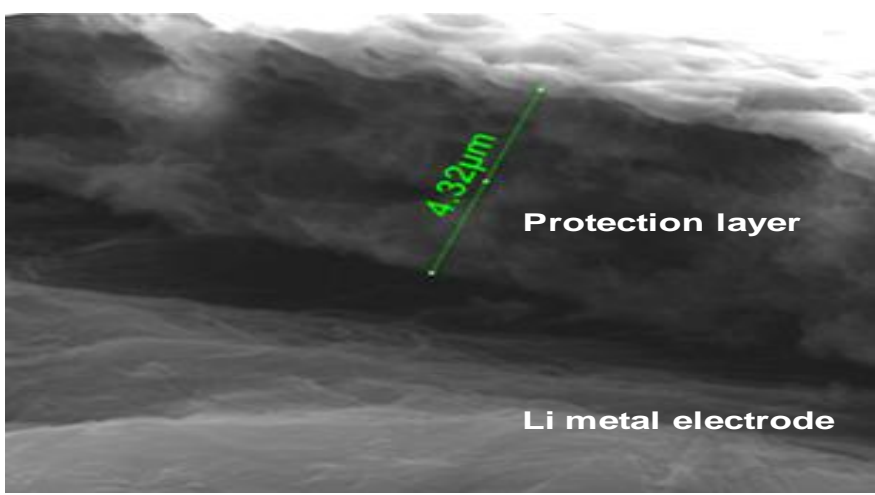
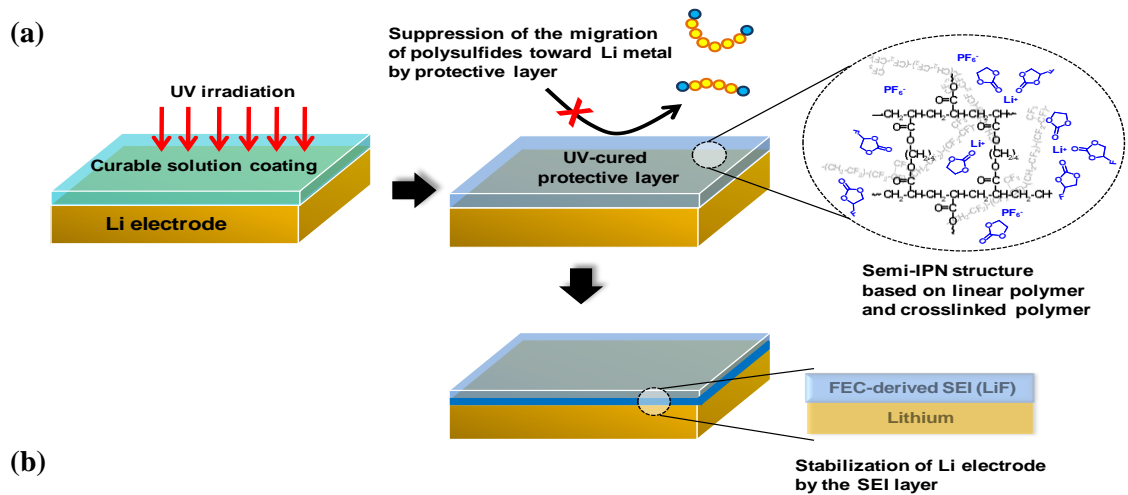


Figure 19. (a) Schematic drawing for the formation and roles of a protective layer on the Li electrode via UV irradiation. (b) SEM image of a protective layer. (c) A Li-S cell with a protective layer.

3. Results and Discussion

3.1. Effect of TEGDME on Li metal

Figure 20 presents the voltage profile for first Li dissolution from the Li electrode in 1M LiPF₆ dissolved in tetra(ethylene glycol) dimethyl ether (TEGDME) used as a solvent for Li-S cells. A sharp decline in the potential between the two Li electrodes was observed after 4 h and the Li symmetrical cell eventually explodes. This result reveals that a TEGDME solvent is not proper to stabilize the Li electrode. Taking this into consideration, functional solvents, which can form stable SEI, should be used. The unique property of fluoroethylene carbonate (FEC) has been identified by the ability to effectively stabilize the Li metal electrode/electrolyte interface.⁷

3.2. Effect of FEC based electrolyte on lithium deposition/dissolution process in Li symmetric cell.

Figure 21 shows the galvanostatic cycling of Li symmetric cells in ethylene carbonate (EC)/ethylmethyl carbonate (EMC)/1M LiPF₆ with and without FEC. The FEC-free electrolyte, Ref, showed a large potential drop and very unstable potential behavior between the two Li electrodes during cycling, and the cell exploded at 10 cycles due to short circuit by dendritic lithium and less effective passivation of the Li electrode. This indicates that the FEC-free electrolyte does not allow reversible deposition and dissolution of Li metal. Interestingly, the FEC-based electrolyte, FEC60, showed a low potential drop and highly stable potential behavior for deposition and dissolution of Li on the Li electrode after 6 cycles, as shown in Fig. 21(b). It is thought that the FEC-derived SEI effectively assists Li migration to the Li electrode surface and permits reversible deposition/dissolution of Li in the Li symmetrical cell. To understand the influence of FEC on the cell resistance, electrochemical impedance measurements of the Li symmetrical cells after 5 and 10 cycles were carried out. Figs. 21(c) and (d) show the cell impedance from three components: the intercept at high frequency for the ohmic resistance of the cell, the impedance associated with Li migration across the SEI, and the resistance for the faradaic charge transfer reaction at low frequency. The FEC-containing electrolyte suppressed increment of the total resistance of the Li symmetrical cell after 5 and 10 cycles, compared to Ref-P. The FEC-containing electrolytes are thought to develop the better passivation on the Li anode, compared to the FEC-free electrolytes. This result is in good agreement with the low potential drop of the Li symmetrical cell cycled in the FEC-containing electrolyte, as shown in Figs. 21(a) and (b).

SEM images of the Li electrode surface after Li deposition and Li dissolution for current density

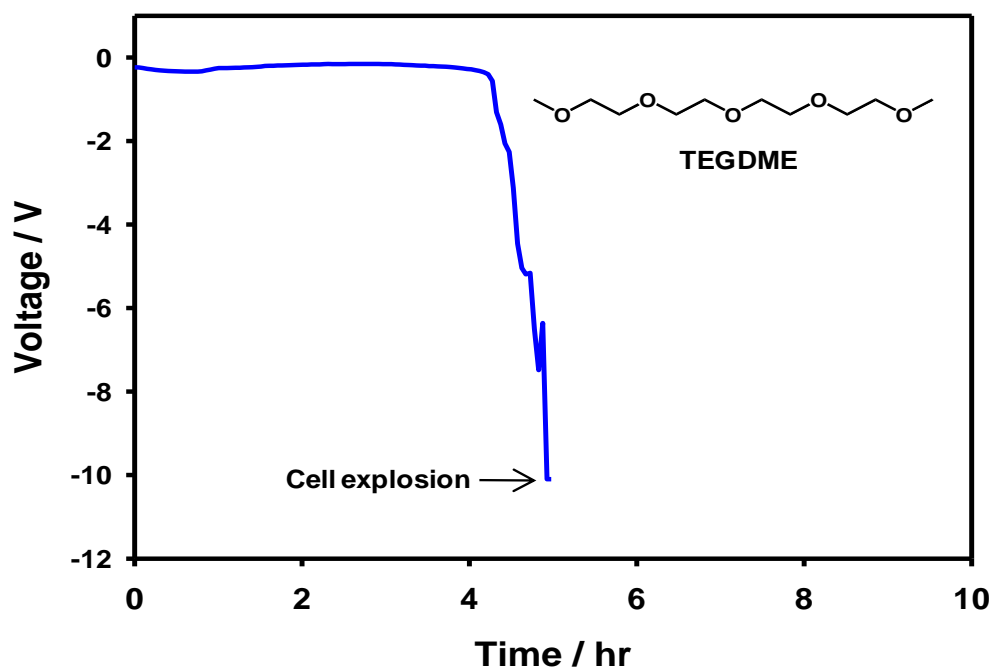


Figure 20. Galvanostatic cycling performance of Li symmetrical cells in TEGDME/1M LiPF₆ at a rate of C/10 during first Li dissolution from the Li electrode.

of 1.5mA cm^{-2} are shown in Figure 22. There was no significant difference between the Li electrodes after Li dissolution in electrolytes with and without FEC, as shown in Figs. 21(a) and (b). On the other hand, it is clearly seen that the size of dendritic Li deposited on the Li electrode surface in the FEC-containing electrolyte is much larger than the Li deposit in the FEC-free electrolyte, as shown in Figs. 21(c) and (d). Li deposition may continuously occur on the specific location of the Li electrode in the FEC-containing electrolyte, and thereby the size of the Li dendrite seems to be expanded. The effect of FEC on the chemical structure of the Li electrode surface was investigated by means of ATR-FTIR spectroscopy. The peaks corresponding to lithium alkylcarbonate (ROCO_2Li) at 1317, 1401, and 1650 cm^{-1} were observed at the Li surface after Li dissolution in Ref, as shown in Fig. 23. ROCO_2Li is formed by reductive decomposition of EC and EMC.⁸² In the case of the FEC-containing electrolyte, no peaks attributed to ROCO_2Li appeared on the Li surface after Li dissolution, as presented in Fig.23. The broad peak around 1800 cm^{-1} originated from polycarbonate produced by FEC decomposition.⁸² The FEC-derived SEI including polycarbonate is expected to mitigate electrochemical decomposition of EC and EMC during Li dissolution from the Li electrode and to assure reversible electrochemical reactions of Li symmetrical cells.

Figure 24 shows the XPS spectra for the surface layer formed on the Li electrodes after Li dissolution in Ref and FEC60. The F 1s XPS spectra display a convolution of two peaks as well as the fitting curves for electrolytes with and without FEC. The peak centered at 687 eV is assigned to LiF and the peak at 689.5 eV corresponds to Li_xPF_y and Li_xPOF_y .⁸²⁻⁸⁵ It is clear that the peak intensity corresponding to LiF increased in the FEC-based electrolyte. The proportion of LiF was calculated on the basis of a quantitative analysis of the XPS spectra. The electrochemical decomposition of FEC-free electrolyte produced 67% of LiF in the SEI, while 88% of LiF was formed in FEC60 electrolyte. LiF can be generated via the electrochemical reactions of PF_5 and PF_6^- with Li, and the electrochemical decomposition of FEC.^{75,85} From these results of the XPS studies, we confirmed that relatively high concentration of LiF in FEC60 is ascribed to the FEC decomposition. It is believed that stable cycling of the Li symmetrical cell with FEC60 electrolyte of Fig. 17(b) is achieved by this LiF-based SEI.

Figure 25 shows images of the lithium electrode surface dissolved in electrolytes with and without FEC by time of flight secondary ion mass spectrometry (ToF-SIMS) negative ion mode measurements. The maximum intensity of secondary ions is shown in white (the color bar is an intensity scale). The intensity of the F^- ion related to LiF is stronger in the image of the Li electrode surface dissolved in FEC60 electrolyte, because LiF generated by FEC decomposition mainly covers the Li surface, as presented in Fig. 24. This agrees well with the XPS results, indicating the formation of LiF on the Li electrode surface cycled in FEC60.

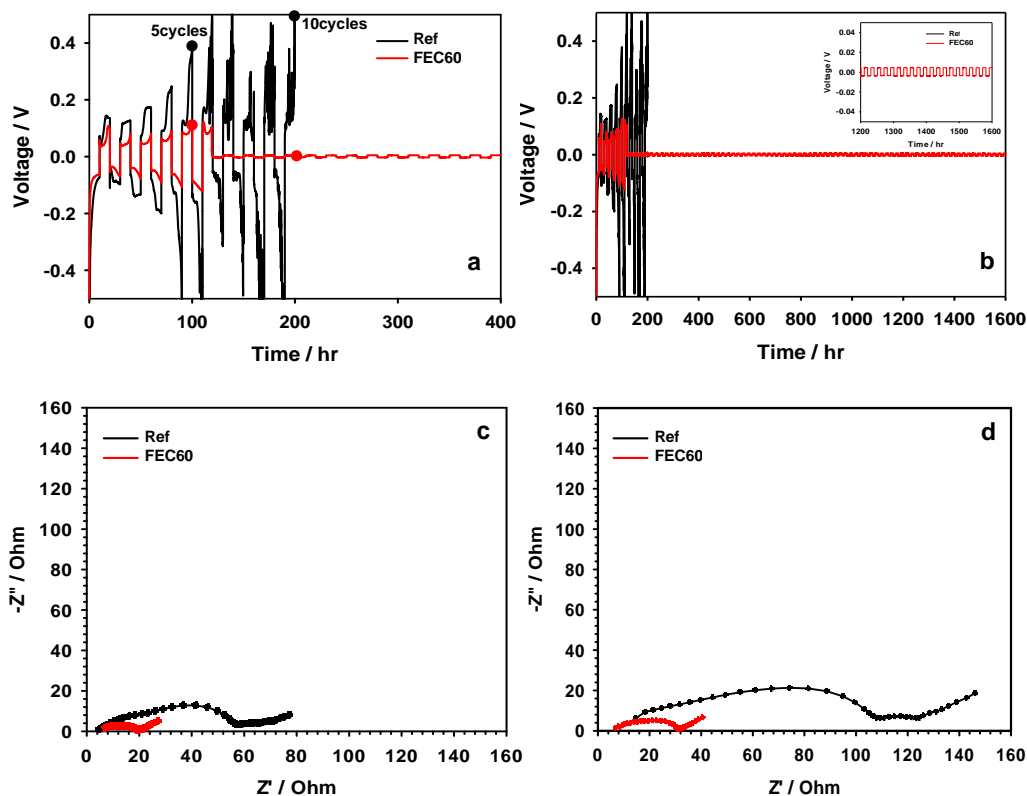


Figure 21. Galvanostatic cycling performance of Li symmetrical cells in Ref and FEC60 electrolytes at a rate of C/10 (a) during 10 cycles. (b) during 80 cycles. The inset is the enlarged zone from 60 to 80 cycles. 25% of Li from the Li counter electrode migrates to the Li working electrode in the Li/electrolyte/Li cell during Li deposition. (c) Impedance spectra of Li symmetrical cells after 5 cycles, (d) Impedance spectra of Li symmetrical cells after 10 cycles.

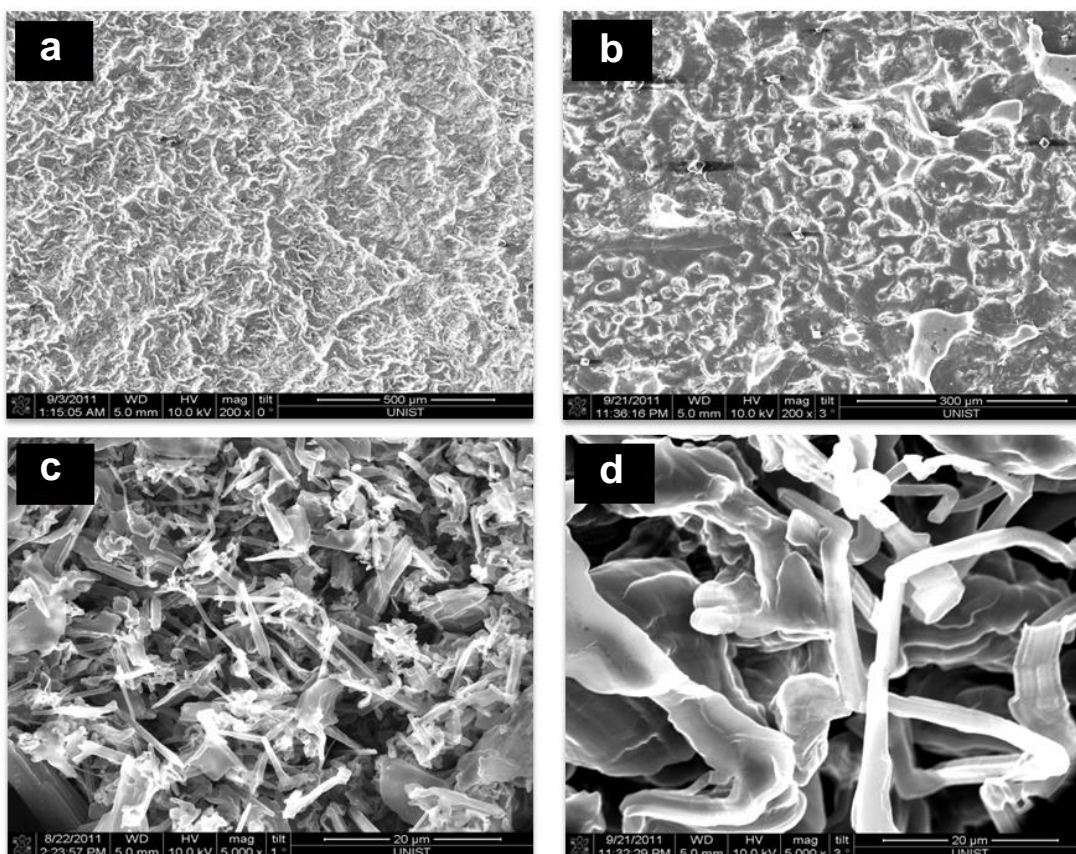


Figure 22. SEM images of the Li electrode surface after Li dissolution in (a) Ref. (b) FEC60, after Li deposition in (c) Ref. (d) FEC60.

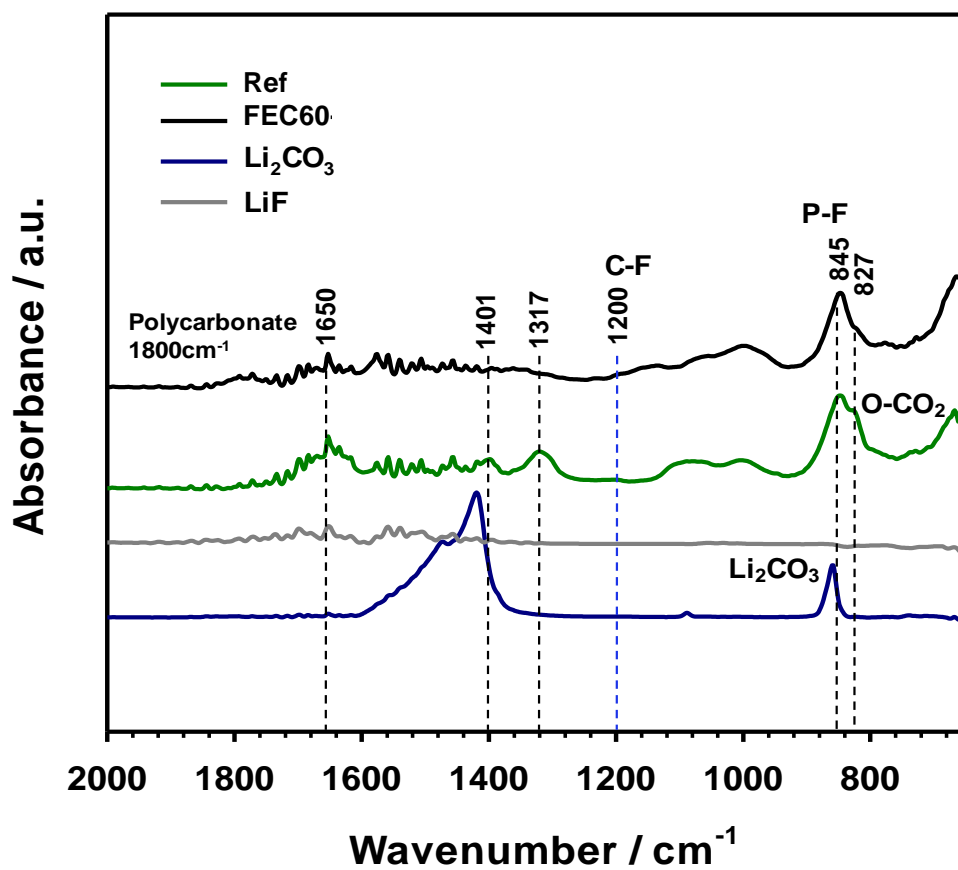


Figure 23. ATR-FTIR spectra of the Li electrode surface after Li dissolution in two electrolyte solutions.

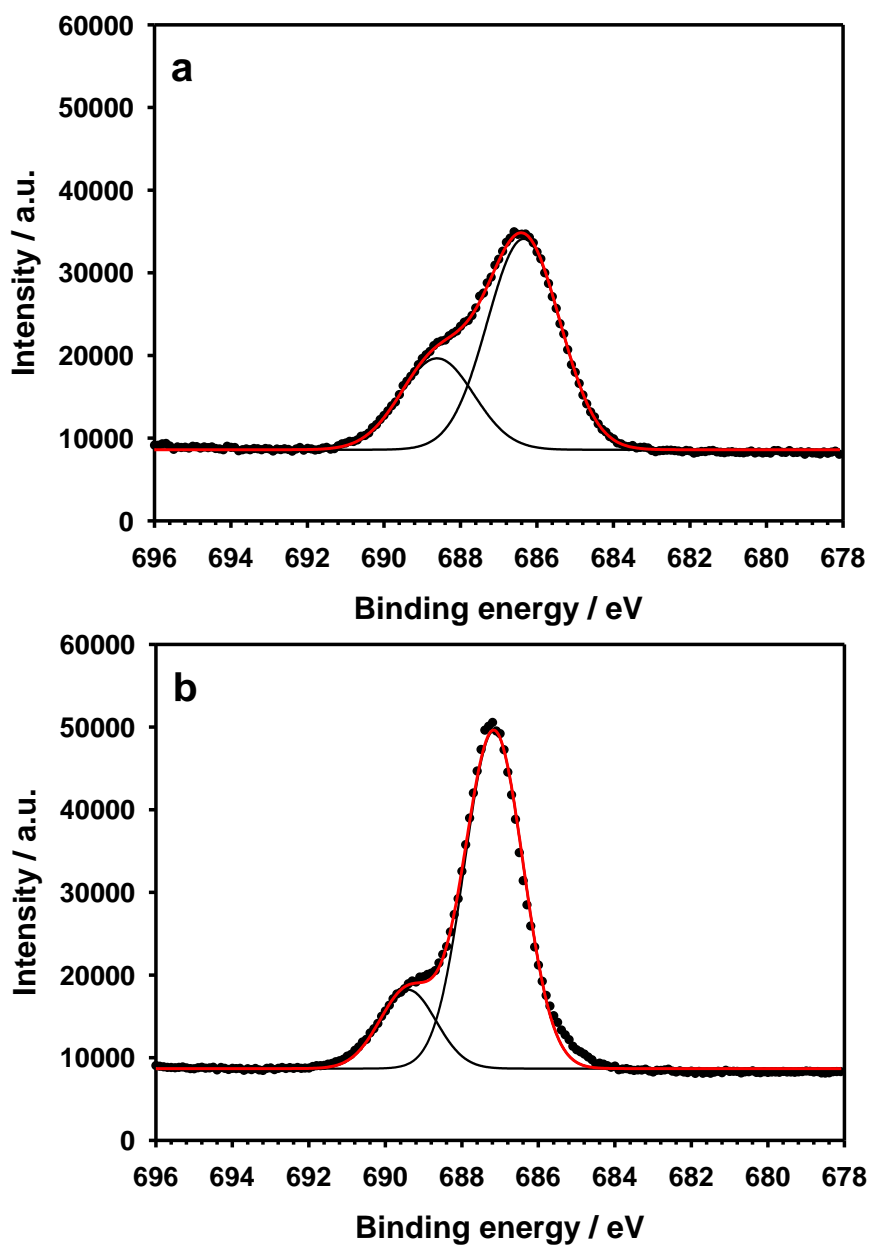


Figure 24. F1s high-resolution XPS spectra of surface films formed on Li electrode surface after Li dissolution in (a) Ref, (b) FEC60 at 30°C. Red lines are curve fitting results.

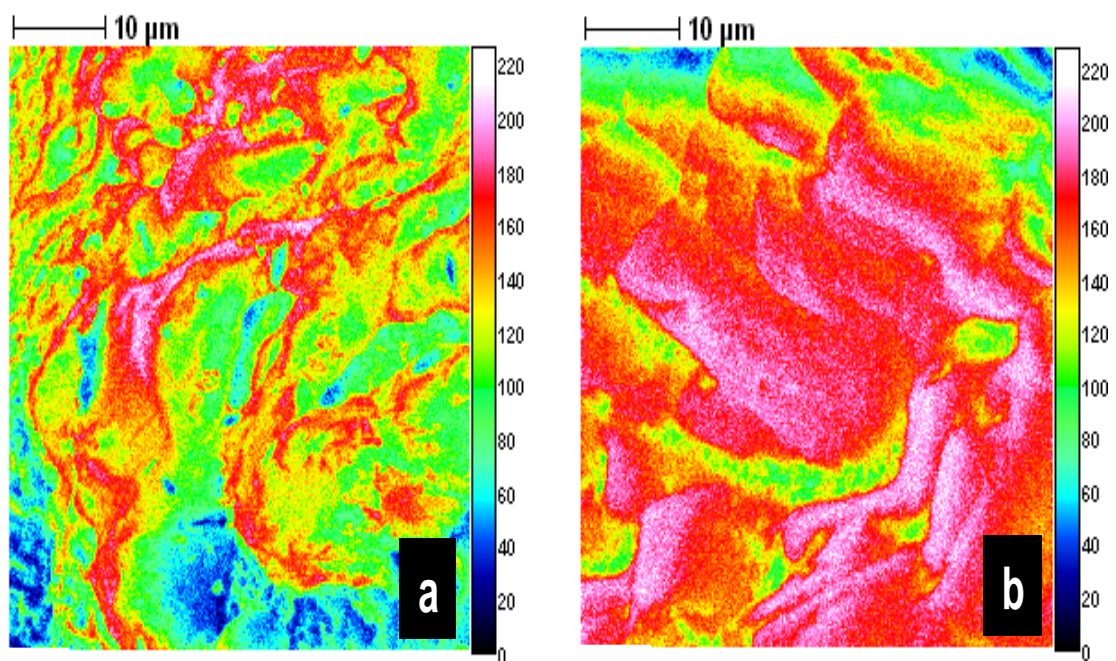


Figure 25. ToF-SIMS F⁻ ion maps of the Li electrode surface after dissolution in (a) Ref, (b) FEC60.

3.3. Effect of protection layer on charge & discharge performance of Li-S cell

Since carbonate solvents such as FEC, which could stabilize the Li metal, may impede electrochemical reduction of elemental sulfur to lithium polysulfides,⁸⁶ the polymer film with FEC60 was formed on the Li electrode to physically separate it with bulk electrolyte. This method seems to be the reasonable way to minimize the effect of an additive for the Li metal on the electrochemical reaction of sulfur cathode.

Figure 26(a) displays the voltage profiles of Li-S cells with and without a protective layer at precycle. Two different protective layers based on a semi-IPN structure were formed on the lithium electrode by UV irradiation and its composition was summarized in Table 3. It is expected that the protective layer hinders the contact of polysulfides with the Li electrode as displayed in Fig. 19(a). The cell with the protection layer 2 exhibited slightly lower discharge capacity of 1029 mAh g⁻¹ than 1183 mAh g⁻¹ of the cell with the non-protected Li anode at precycle. This is likely because the presence of protection layer 2 causes an increase in the resistance of the cell. The cell with the protection layer 2 was charged to 2.8 V vs. Li/Li⁺ without significant overcharge during precycle, while the cell with the protective layer 1 and without the protective layer showed significant overcharging even at precycle. It is clear that the protection layer with FEC60 effectively retards the migration of soluble polysulfide species to the Li electrode surface, which initiates the shuttle phenomenon. Interestingly, although the protection layer 1 was formed on the Li electrode, significant overcharge took place in a Li-S cell, as shown in Fig. 26. To understand this result, scanning electron microscopy (SEM) observation was carried out in combination with energy dispersive X-ray spectrometer (EDS) mapping. Significant physical fracture of the protection layer 1 with TEGDME was observed by the non-uniform Li deposition during charging process, as shown in Fig. 27(a). This indicates that TEGDME in the protection layer 1 does not form a stable SEI and thereby uneven Li deposition takes place on the Li electrode. It is likely that the protection layer 1 does not endure the stress by this uneven Li deposition and is broken down. By contrast, the protection layer 2 with FEC60 maintained its structure. This result provides persuasive evidence that FEC solvent forms a stable SEI on the Li electrode and leads to the uniform Li deposition during charge process.

In order to investigate the effect of solvent species in the protection layer on the migration of soluble lithium polysulfides into that layer, the EDS mapping observation was performed, as shown in Fig. 27(c) and (d). More intense and bright green color indicating relatively high concentration of the sulfur element appeared across the surface of the protection layer 1 with a TEGDME solvent. This is likely because soluble lithium polysulfide species (Li₂S_n, n = 4~6) are more easily penetrated into the protection layer 1 with a TEGDME solvent compared to the protection layer 2 with FEC. From the EDS mapping images, it is confirmed that long chain polysulfides are more soluble in a TEGDME

solvent than in FEC-based solvent.

To investigate the effect of the protection layer on the surface morphology and composition change of the Li metal electrodes after precycle, the SEM observation combined with the EDS spectra were performed. It is clearly seen that non-protected Li metal electrode is entirely covered with a nonuniform surface film consisting of sulfur, phosphorous, fluorine, oxygen and carbon, as shown in Fig. 28(a). Pronounced sulfur signal on the Li metal surface may be attributed to insoluble Li_2S_2 or Li_2S formed by the reaction between long chain polysulfides and the Li metal. On the other hand, the Li metal electrode with the protection layer 2 exhibited considerably reduced sulfur signal in Fig. 28(b). This result suggests that the presence of the protection layer 2 with FEC-based electrolyte between an Li metal electrode and bulk electrolyte effectively suppresses the migration of polysulfides toward an Li metal electrode.

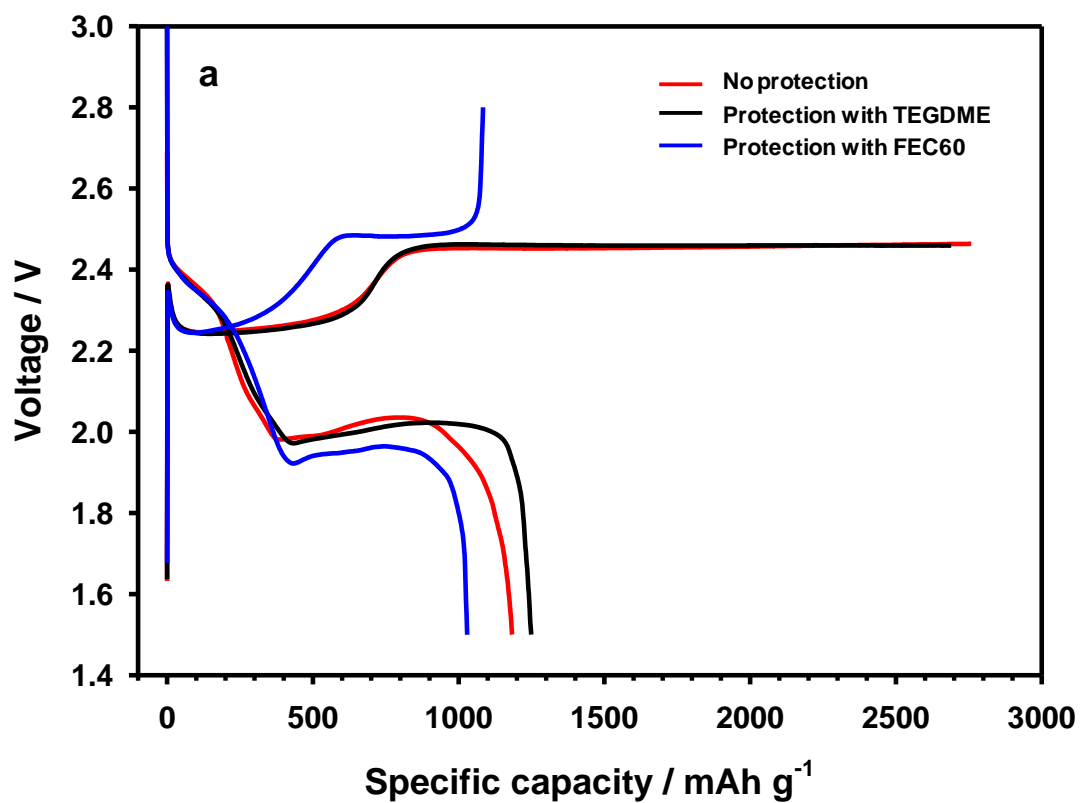


Figure 26. Electrochemical performance of the Li-S cells during galvanostatic cycling at 30°C. (a) Voltage profiles, (b) Coulombic efficiency, (c) Discharge capacity.

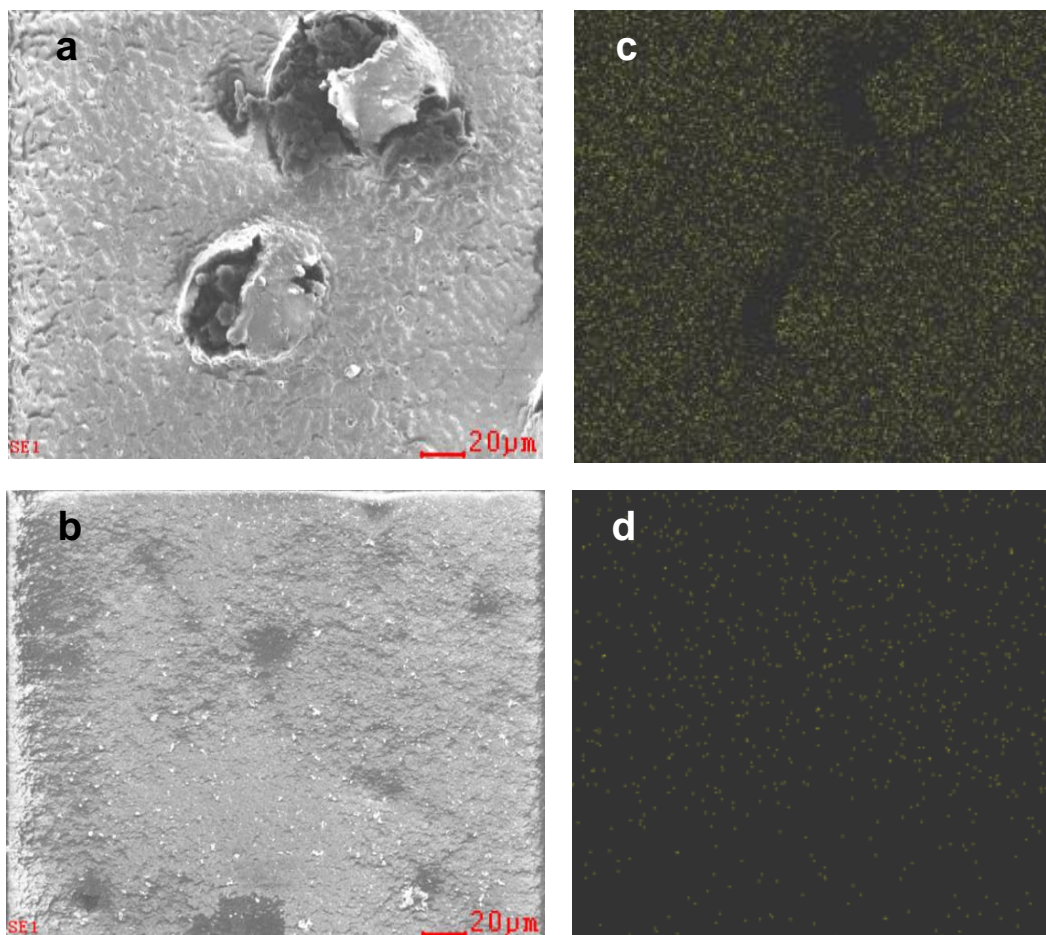


Figure 27. SEM images of the surface of the protection layer with (a) TEGDME electrolyte, (b) FEC60 electrolyte. EDS mapping results for the surface of the protection layer with (a) TEGDME electrolyte, (b) FEC60 electrolyte.

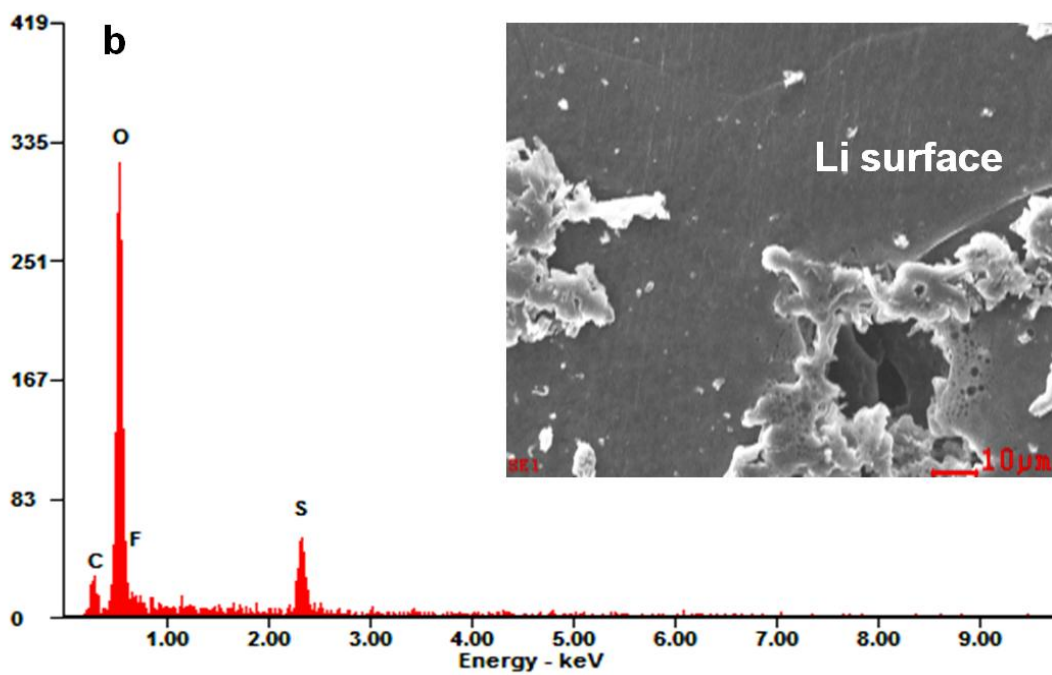
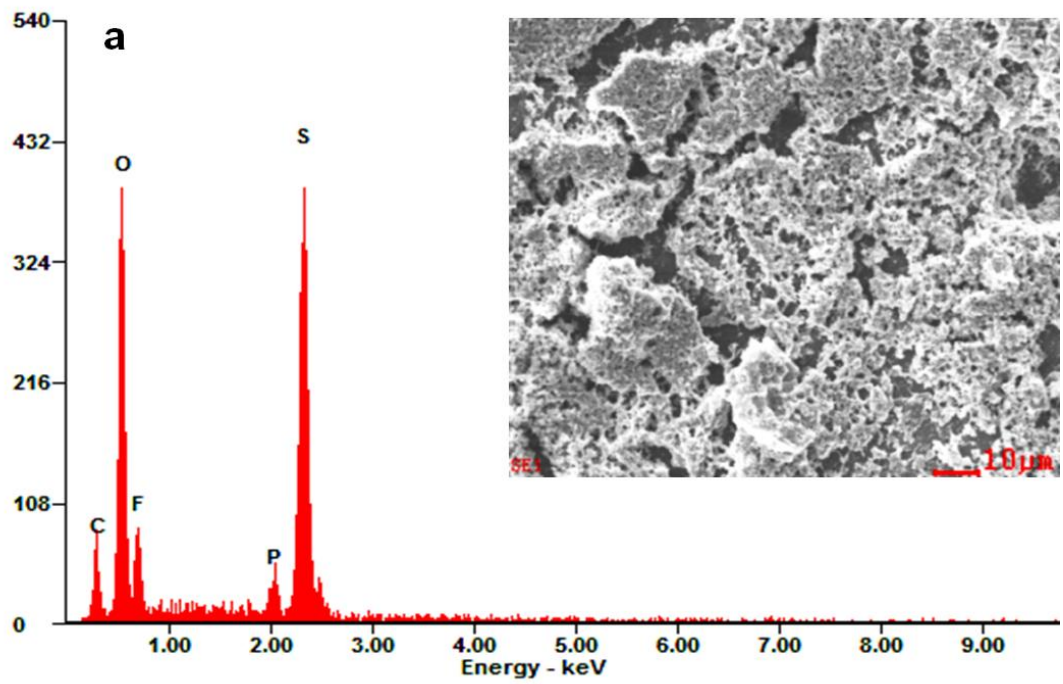


Figure 28. SEM images and EDS spectra of non-protected Li and protected Li surface .

4. Conclusions

The positive effect of FEC on the galvanostatic cycling of Li metal electrodes was described. ATR-FTIR, XPS, and ToF-SIMS studies confirmed that the surface film formed on the Li electrode surface cycled in FEC-containing electrolytes mostly consists of LiF, whereas in the FEC-free electrolytes, linear alkyl carbonates (ROCO₂Li), Li₂CO₃, Li_xPF_y, and Li_xPOF_y, are produced as the dominant species. The protective layer with FEC-based electrolyte significantly suppressed overcharging indicating the shuttle phenomenon of soluble lithium polysulfide.

References

1. Nagaura, T.; Tozawa, K. Lithium ion rechargeable battery. *Prog. Batteries Sol. Cells*, **1990**, *9*, 209-217.
2. Tarascon, J. M.; Armand, M., Issues and challenges facing rechargeable lithium batteries. *Nature* **2001**, *414* (6861), 359-67.
3. Schalkwijk, W. V.; Scrosati, B.: *Advances in Lithium-Ion Batteries*; Kluwer Academic/ Plenum Publishers: New York , 2002.
4. Nazri, G. A.; Pistoia, G.: *Lithium Batteries: Science and Technology*, Springer, 2003.
5. Armand, M., In *Materials for Advanced Batteries*; Murphy, D. W., Broadhead, J., Steele, B. C. H.,(Eds); Plenum Press: New York, 1980, p. 145.
6. Xu, K., Nonaqueous liquid electrolytes for lithium-based rechargeable batteries. *Chemical reviews* **2004**, *104* (10), 4303-417
7. Ji, L. W.; Rao, M. M.; Aloni, S.; Wang, L.; Cairns, E. J.; Zhang, Y. G., Porous carbon nanofiber-sulfur composite electrodes for lithium/sulfur cells. *Energy Environ. Sci.* **2011**, *4* (12), 5053-5059.
8. Peramunage, D.; Licht, S., A solid sulfur cathode for aqueous batteries. *Science* **1993**, *261* (5124), 1029-32.
9. Ji, X. L.; Nazar, L. F., Advances in Li-S batteries. *J. Mater. Chem.* **2010**, *20* (44), 9821-9826.
10. Shim, J.; Striebel, K. A.; Cairns, E. J., The lithium/sulfur rechargeable cell - Effects of electrode composition and solvent on cell performance. *J. Electrochem. Soc.* **2002**, *149* (10), A1321-A1325.
11. Gao, X. P.; Yang, H. X., Multi-electron reaction materials for high energy density batteries. *Energy Environ. Sci.* **2010**, *3* (2), 174-189.
12. Ji, X.; Lee, K. T.; Nazar, L. F., A highly ordered nanostructured carbon-sulphur cathode for lithium-sulphur batteries. *Nat Mater* **2009**, *8* (6), 500-6.

13. Jin, B.; Kim, J. U.; Gu, H. B., Electrochemical properties of lithium-sulfur batteries. *J. Power Sources* **2003**, *117* (1-2), 148-152.
14. Wei, S. C.; Zhang, H.; Huang, Y. Q.; Wang, W. K.; Xia, Y. Z.; Yu, Z. B., Pig bone derived hierarchical porous carbon and its enhanced cycling performance of lithium-sulfur batteries. *Energy Environ. Sci.* **2011**, *4* (3), 736-740.
15. Hassoun, J.; Scrosati, B., A high-performance polymer tin sulfur lithium ion battery. *Angewandte Chemie* **2010**, *49* (13), 2371-4.
16. Cheon, S. E.; Ko, K. S.; Cho, J. H.; Kim, S. W.; Chin, E. Y.; Kim, H. T., Rechargeable lithium sulfur battery - I. Structural change of sulfur cathode during discharge and charge. *J. Electrochem. Soc.* **2003**, *150* (6), A796-A799.
17. Etacheri, V.; Marom, R.; Elazari, R.; Salitra, G.; Aurbach, D., Challenges in the development of advanced Li-ion batteries: a review. *Energy Environ. Sci.* **2011**, *4* (9), 3243-3262.
18. Yang, Y.; McDowell, M. T.; Jackson, A.; Cha, J. J.; Hong, S. S.; Cui, Y., New nanostructured Li₂S/silicon rechargeable battery with high specific energy. *Nano letters* **2010**, *10* (4), 1486-91.
19. Rauh, R. D.; Shuker, F. S.; Marston, J. M.; Brummer, S. B., FORMATION OF LITHIUM POLYSULFIDES IN APROTIC MEDIA. *Journal of Inorganic & Nuclear Chemistry* **1977**, *39* (10), 1761-1766.
20. John A. Dean.: *Lange's Handbook of Chemistry*, 3rd ed.; McGraw-Hill: New York, 1985, pp. 3-5.
21. Cheon, S. E.; Ko, K. S.; Cho, J. H.; Kim, S. W.; Chin, E. Y.; Kim, H. T., Rechargeable lithium sulfur battery - II. Rate capability and cycle characteristics. *J. Electrochem. Soc.* **2003**, *150* (6), A800-A805.
22. Jeon, B. H.; Yeon, J. H.; Kim, K. M.; Chung, I. J., Preparation and electrochemical properties of lithium-sulfur polymer batteries. *J. Power Sources* **2002**, *109* (1), 89-97.
23. Yamin, H.; Peled, E., Electrochemistry of a nonaqueous lithium-sulfur cell. *Journal of Power Sources*, **1998**, *9*, 281-287.

24. Yamin, H.; Gorenshstein, A.; Penciner, J.; Sternberg, Y.; Peled, E., LITHIUM SULFUR BATTERY - OXIDATION REDUCTION-MECHANISMS OF POLYSULFIDES IN THF SOLUTIONS. *J. Electrochem. Soc.* **1988**, *135* (5), 1045-1048.
25. Yamaki, J. I.; Tobishima, S. I.; Sakurai, Y.; Saito, K. I.; Hayashi, K., Safety evaluation of rechargeable cells with lithium metal anodes and amorphous V₂O₅ cathodes. *J. Appl. Electrochem.* **1998**, *28* (2), 135-140.
26. He, G.; Ji, X. L.; Nazar, L., High "C" rate Li-S cathodes: sulfur imbibed bimodal porous carbons. *Energy Environ. Sci.* **2011**, *4* (8), 2878-2883.
27. Kumaresan, K.; Mikhaylik, Y.; White, R. E., A mathematical model for a lithium-sulfur cell. *J. Electrochem. Soc.* **2008**, *155* (8), A576-A582.
28. Ragnar P. Tischer., *The sulfur electrode*, Academic press, 1983, pp.223-224.
29. Cairns, E.J. & Steunenber, R.K., Progress in *High Temp. Phys. Chem.*(3rd ed), 5, New York, 63, 1973.
30. Rudolf Kummer, Otto Leman, and Heinz-Walter Schenider., US Patent No.3,413, 150, 1968.
31. May-Ying Chu., US Patent No. 5, 523, 007, 1996.
32. May-Ying Chu., US Patent No. 5, 523, 179, 1996
33. Lutgard C. Dejouge, Steven J. Visco, Catherine C. Mailhe, and Michael B. Armand., US Patent No. 4,833,048, 1989.
34. DeGott, P. *Polymere Carbone-Soufre Synthese et Proprietes Electrochimiques*. Doctorial thesis, at l'Institut National Polytechnique de Grenoble, pp. 117-119, 1986.
35. Steven J.Visco., May-Ying Chu, and Lutgard C. De Jonghe., US Patent No. 5,882,812, 1999.
36. May-Ying Chu., US Patent No. 5, 686, 201, 1997.

37. May-Ying Chu., US Patent No. 5, 789, 108, 1998.
38. Licht, S., Aluminum/sulfur battery discharge in the high current domain. *J. Electrochem. Soc.* **1997**, *144* (6), L133-L136.
39. May-Ying Chu, Lutgard C. De Jonghe, Steven J. Visco, and Bruce D. Kate., US Patent No. 6,030,720, 2000.
40. Terje Absjorn Skotheim., US Patent No, 5, 648, 187, 1997.
41. James R. Akridge, Yuriy Mikhaylik., *Lithium-Sulfur Secondary Battery: Chemistry and Practical System Performance*, PBFC-2 Las Vegas, Nevada, USA, June 12-17. 2005
42. Rao. M. L. B., U.S. Patent No. 3, 13, 154, 1968.
43. Nole D., Moss. V., U.S. Patent No. 3, 532, 543, 1970.
44. Merritt, M. V.; Sawyer, D. T., ELECTROCHEMICAL REDUCTION OF ELEMENTAL SULFUR IN APROTIC SOLVENTS . FORMATION OF A STABLE S₈-SPECIES. *Inorg. Chem.* **1970**, *9* (2), 211-&.
45. Martin, R. P., Doub Jr., W. H., Roberts Jr., J. L. & Sawyer, D. T., Further studies of the electrochemical reduction of sulfur in aprotic solvents. *Inorganic Chemistry.*, **1973**, *12*, 1921.
46. Aggarwal, R. L.; Farrar, L. W.; Polla, D. L., Measurement of the absolute Raman scattering cross sections of sulfur and the standoff Raman detection of a 6-mm-thick sulfur specimen at 1500 m. *J. Raman Spectrosc.* **2011**, *42* (3), 461-464.
47. Daly, F. P.; Brown, C. W., RAMAN-SPECTRA OF SODIUM TETRASULFIDE IN PRIMARY AMINES - EVIDENCE FOR S₄²⁻ AND S₈^{N-} IN RHOMBIC SULFUR-AMINE SOLUTIONS. *J. Phys. Chem.* **1975**, *79* (4), 350-354.
48. Dubois, P.; Lelieur, J. P.; Lepoutre, G., IDENTIFICATION AND CHARACTERIZATION OF LITHIUM POLYSULFIDES IN SOLUTION IN LIQUID-AMMONIA. *Inorg. Chem.* **1988**, *27* (1), 73-80.

49. Tatsumi, K.; Kawaguchi, H.; Inoue, K.; Tani, K.; Cramer, R. E., LITHIUM CATIONS TIGHTLY BOUND TO POLYCHALCOGENIDES - SYNTHESIS AND SOLID-STATE STRUCTURES OF $\text{Li}_2\text{S}_6(\text{TEEDA})_2$, $\text{Li}_2\text{S}_4(\text{PMDETA})_2$, AND $\text{Li}_2\text{S}_5(\text{PMDETA})_2$. *Inorg. Chem.* **1993**, 32 (20), 4317-4323.
50. Chivers, T., UBIQUITOUS TRISULFUR RADICAL ION S_3 . *Nature* **1974**, 252 (5478), 32-33.
51. Rauh, R. D.; Abraham, K. M.; Pearson, G. F.; Surprenant, J. K.; Brummer, S. B., LITHIUM-DISSOLVED SULFUR BATTERY WITH AN ORGANIC ELECTROLYTE. *J. Electrochem. Soc.* **1979**, 126 (4), 523-527.
52. Yuan, L. X.; Qiu, X. P.; Chen, L. Q.; Zhu, W. T., New insight into the discharge process of sulfur cathode by electrochemical impedance spectroscopy. *J. Power Sources* **2009**, 189 (1), 127-132.
53. Wang, Y.; Huang, Y. Q.; Wang, W. K.; Huang, C. J.; Yu, Z. B.; Zhang, H.; Sun, J.; Wang, A. B.; Yuan, K. G., Structural change of the porous sulfur cathode using gelatin as a binder during discharge and charge. *Electrochim. Acta* **2009**, 54 (16), 4062-4066.
54. Nelson, J.; Misra, S.; Yang, Y.; Jackson, A.; Liu, Y. J.; Wang, H. L.; Dai, H. J.; Andrews, J. C.; Cui, Y.; Toney, M. F., In Operando X-ray Diffraction and Transmission X-ray Microscopy of Lithium Sulfur Batteries. *J. Am. Chem. Soc.* **2012**, 134 (14), 6337-6343.
55. Choi, Y. J.; Chung, Y. D.; Baek, C. Y.; Kim, K. W.; Ahn, H. J.; Ahn, J. H., Effects of carbon coating on the electrochemical properties of sulfur cathode for lithium/sulfur cell. *J. Power Sources* **2008**, 184 (2), 548-552.
56. Chang, D. R.; Lee, S. H.; Kim, S. W.; Kim, H. T., Binary electrolyte based on tetra(ethylene glycol) dimethyl ether and 1,3-dioxolane for lithium-sulfur battery. *J. Power Sources* **2002**, 112 (2), 452-460.
57. Caleman, C.; van Maaren, P. J.; Hong, M. Y.; Hub, J. S.; Costa, L. T.; van der Spoel, D., Force Field Benchmark of Organic Liquids: Density, Enthalpy of Vaporization, Heat Capacities, Surface Tension, Isothermal Compressibility, Volumetric Expansion Coefficient, and Dielectric Constant. *J. Chem. Theory Comput.* **2012**, 8 (1), 61-74.

58. Sciamanna, S. F.; Lynn, S., SULFUR SOLUBILITY IN PURE AND MIXED ORGANIC-SOLVENTS. *Ind. Eng. Chem. Res.* **1988**, 27 (3), 485-491.
59. Ikeda, H., Saito, T. & Tamura, H., in *Proc. Manganese Dioxide Symposium*, Vol 1(eds Kozawa, A. & Brodd, R.H.): IC sample Office, Cleveland, 1975, OH.
60. Murphy, D. W.; Disalvo, F. J.; Carides, J. N.; Waszczak, J. V., TOPOCHEMICAL REACTIONS OF RUTILE RELATED STRUCTURES WITH LITHIUM. *Mater. Res. Bull.* **1978**, 13 (12), 1395-1402.
61. Lazzari, M.; Scrosati, B., CYCLABLE LITHIUM ORGANIC ELECTROLYTE CELL BASED ON 2 INTERCALATION ELECTRODES. *J. Electrochem. Soc.* **1980**, 127 (3), 773-774.
62. Armand, M., Chabagno, J. M., Duclot, M. J., in *Fast Ion Transport in Solids Electrodes and Electrolytes* (eds Vashishta, P., Mundy, J.-N. & Shenoy, G. K.) 131-136 (North-Holland, Amsterdam), 1979.
63. Kelly, I. E., Owen, J. R. & Steel, B. H., Poly(ethyleneoxide) electrolytes for operation at near room temperature. *J. Power Sources* **1985**, 14, 13-21; *Interfacial Electrochem.* **1984**, 168, 467.
64. Yamin, H.; Penciner, J.; Gorenshain, A.; Elam, M.; Peled, E., THE ELECTROCHEMICAL-BEHAVIOR OF POLYSULFIDES IN TETRAHYDROFURAN. *J. Power Sources* **1985**, 14 (1-3), 129-134.
65. Marmorstein, D.; Yu, T. H.; Striebel, K. A.; McLarnon, F. R.; Hou, J.; Cairns, E. J., Electrochemical performance of lithium/sulfur cells with three different polymer electrolytes. *J. Power Sources* **2000**, 89 (2), 219-226.
66. Takehara, Z.; Ogumi, Z.; Uchimoto, Y.; Yasuda, K.; Yoshida, H., MODIFICATION OF LITHIUM ELECTROLYTE INTERFACE BY PLASMA POLYMERIZATION OF 1,1-DIFLUOROETHENE. *J. Power Sources* **1993**, 44 (1-3), 377-383.
67. Ogumi, Z.; Uchimoto, Y.; Endo, E.; Takehara, Z., IONICALLY CONDUCTIVE THIN POLYMER-FILMS PREPARED BY PLASMA POLYMERIZATION .8. VAPOR-PHASE PREPARATION OF SOLID POLYMER ELECTROLYTES COMPOSED OF PLASMA

POLYMER AND VAPOR-DEPOSITED LITHIUM IODIDE COMPLEX. *Electrochim. Acta* **1992**, 37 (9), 1483-1486.

68. Osaka, T.; Momma, T.; Matsumoto, Y.; Uchida, Y., Surface characterization of electrodeposited lithium anode with enhanced cycleability obtained by CO₂ addition. *J. Electrochem. Soc.* **1997**, 144 (5), 1709-1713.

69. Osaka, T.; Momma, T.; Matsumoto, Y.; Uchida, Y., Effect of carbon dioxide on lithium anode cycleability with various substrates. *J. Power Sources* **1997**, 68 (2), 497-500.

70. Visco, S.J. *Power2000 presentation of PolyPlus Battery Company.*

71. Choi, N. S.; Lee, Y. M.; Park, J. H.; Park, J. K., Interfacial enhancement between lithium electrode and polymer electrolytes. *J. Power Sources* **2003**, 119, 610-616.

72. Choi, N. S.; Lee, Y. M.; Seol, W.; Lee, J. A.; Park, J. K., Protective coating of lithium metal electrode for interfacial enhancement with gel polymer electrolyte. *Solid State Ion.* **2004**, 172 (1-4), 19-24.

73. Choi, N. S.; Lee, Y. M.; Cho, K. Y.; Ko, D. H.; Park, J. K., Protective layer with oligo(ethylene glycol) borate anion receptor for lithium metal electrode stabilization. *Electrochem. Commun.* **2004**, 6 (12), 1238-1242.

74. Lee, Y. M.; Choi, N. S.; Park, J. H.; Park, J. K., Electrochemical performance of lithium/sulfur batteries with protected Li anodes. *J. Power Sources* **2003**, 119, 964-972.

75. Choi, N. S.; Yew, K. H.; Lee, K. Y.; Sung, M.; Kim, H.; Kim, S. S., Effect of fluoroethylene carbonate additive on interfacial properties of silicon thin-film electrode. *J. Power Sources* **2006**, 161 (2), 1254-1259.

76. Sethuraman, V. A.; Kowolik, K.; Srinivasan, V., Increased cycling efficiency and rate capability of copper-coated silicon anodes in lithium-ion batteries. *J. Power Sources* **2011**, 196 (1), 393-398.

77. McMillan, R.; Slegel, H.; Shu, Z. X.; Wang, W. D., Fluoroethylene carbonate electrolyte and its use in lithium ion batteries with graphite anodes. *J. Power Sources* **1999**, 81, 20-26.

78. Mogi, R.; Inaba, M.; Jeong, S. K.; Iriyama, Y.; Abe, T.; Ogumi, Z., Effects of some organic additives on lithium deposition in propylene carbonate. *J. Electrochem. Soc.* **2002**, *149* (12), A1578-A1583.
79. Abe, T.; Sagane, F.; Ohtsuka, M.; Iriyama, Y.; Ogumi, Z., Lithium-ion transfer at the interface between lithium-ion conductive ceramic electrolyte and liquid electrolyte - A key to enhancing the rate capability of lithium-ion batteries. *J. Electrochem. Soc.* **2005**, *152* (11), A2151-A2154.
80. Jung, C., Electrochemical absorption effect of BF₄ anion salt on SEI layer formation. *Solid State Ion.* **2008**, *179* (27-32), 1717-1720.
81. Profatilova, I. A.; Kim, S. S.; Choi, N. S., Enhanced thermal properties of the solid electrolyte interphase formed on graphite in an electrolyte with fluoroethylene carbonate. *Electrochim. Acta* **2009**, *54* (19), 4445-4450.
82. Etacheri, V.; Haik, O.; Goffer, Y.; Roberts, G. A.; Stefan, I. C.; Fasching, R.; Aurbach, D., Effect of Fluoroethylene Carbonate (FEC) on the Performance and Surface Chemistry of Si-Nanowire Li-Ion Battery Anodes. *Langmuir* **2012**, *28* (1), 965-976.
83. Nakai, H.; Kubota, T.; Kita, A.; Kawashima, A., Investigation of the Solid Electrolyte Interphase Formed by Fluoroethylene Carbonate on Si Electrodes. *J. Electrochem. Soc.* **2011**, *158* (7), A798-A801.
84. Eriksson, T.; Andersson, A. M.; Gejke, C.; Gustafsson, T.; Thomas, J. O., Influence of temperature on the interface chemistry of Li_xMn₂O₄ electrodes. *Langmuir* **2002**, *18* (9), 3609-3619.
85. Nakai, H.; Kubota, T.; Kita, A.; Kawashima, A., Investigation of the Solid Electrolyte Interphase Formed by Fluoroethylene Carbonate on Si Electrodes. *J. Electrochem. Soc.* **2011**, *158* (7), A798-A801.
86. He, X. M.; Pu, W. H.; Ren, J. G.; Wang, L.; Wang, J. L.; Jiang, C. Y.; Wan, C. R., Charge/discharge characteristics of sulfur composite cathode materials in rechargeable lithium batteries. *Electrochim. Acta* **2007**, *52* (25), 7372-7376.

